A brainstem circuit for coordinated pain-control

Mark Hoon (mhoon@dir.nidcr.nih.gov)
NIH https://orcid.org/0000-0002-8794-1684
Xinglong Gu

Article

Keywords: brainstem, circuit, coordinated, pain-control

Posted Date: October 30th, 2020

DOI: https://doi.org/10.21203/rs.3.rs-94825/v1

A brainstem circuit for coordinated pain-control

Authors: Xinglong Gu[1] and Mark A. Hoon[1*]

Affiliations: [1]Molecular Genetics Section, National Institute of Dental and Craniofacial Research/NIH, 35 Convent Drive, Bethesda, MD 20892, USA

[*]To whom correspondence should be addressed, email mark.hoon@nih.gov

Abstract

Supraspinal brain regions are involved in modifying nociceptive signals in response to environmental stimuli and stressors including mechanisms that elevate thresholds to noxious stimuli (pain suppression). However, details such as the cells, the circuits, and the molecular mechanisms, by which nociceptive responses are suppressed are incompletely understood. Therefore, we searched for unrecognized brain nuclei involved in these processes. Examination of neurons activated by noxious stimuli revealed catecholaminergic neurons in the caudal ventrolateral medulla that were stimulated by multiple noxious challenges. We found that, upon activation, these neurons operate in a diffuse feed-forward inhibitory loop to attenuate nociceptive reflexes via a descending locus coeruleus to spinal cord pathway. Importantly, this circuit is sufficient to attenuate injury induced allodynia and inhibit glucoprivation induced analgesia and is required for counter-stimulus induced analgesia. Our findings molecularly define a component of the brain pain modulatory system which can coordinate antinociceptive responses

Introduction

The perception of pain is dependent on the noxious stimuli, but can be greatly modified by other factors[1-3]. Indeed after severe traumatic injury, pain may not even be apparent[2]. Less extreme settings can also lead to pain modulation including the suppression of pain by stressors such as food-deprivation[4,5], cold-water imersion[6], and noxious stimulation[7]. Pain suppression processes occur through descending pathways directed at the spinal cord (SC) where they are thought to gate the flow of ascending nociceptive signals. These inhibitory circuits use the neurotransmitters, opioids, GABA, serotonin, and noradrenalin (NA) to modulate activity in the SC[8-10] and drugs that target these transmission processes form the basis for many current pain treatments[11].

Noxious stimuli which are harmful or potentially damaging are detected by nociceptive sensory neurons that innervate many target organs. In turn, signals from these sensors are transmitted to the spinal cord (SC) and then conveyed to supraspinal centers where they are processed to produce salient responses. The brainstem contains several ascending and descending nuclei which have major effects on pain responses including the parabrachial nucleus (PbN)[12-17], the locus coeruleus (LC)[18,19], and the rostral ventral medulla (RVM)[10,20-22]. The PbN as well as the thalamus and several other brain nuclei receive input from spinal cord projection neurons. These centers not only relay important somatic information to other brain regions but are part of somatic and autonomic motor circuits that directly control responses to noxious stimulation. On the other hand, both the LC and RVM send descending projections to the spinal cord releasing NA and serotonin respectively.

Although many of the descending inhibitory pathways have been well characterized, the circuit(s) responsible for several types of intrinsic pain modulation are not well understood. Among these, the circuits involved in diffuse noxious inhibitory control (DNIC)[23,24] and for glucoprivation induced analgesia[5] have not been identified. These types of analgesia are thought to originate in the brainstem[5,25,26] and are likely mediated through connections to either the LC or the RVM, or both. However, the precise upstream neural circuits and mechanisms involved are unknown. Therefore, we sought to uncover unrecognized brainstem nuclei for these processes. Our results revealed a previously unappreciated feed-forward inhibitory circuit that can inhibit pain through a medulla to LC to spinal cord pathway.

Results

Catecholaminergic neurons in the ventrolateral medulla are activated by noxious stimuli

To define potential nuclei involved in pain control in the brainstem we searched for cells activated by unilateral injection (in a hind-paw) of capsaicin, a compound known to elicit pain reactions, screening for cfos positive neurons (a marker for neuronal activation). We found one ensemble of activated neurons in the caudal ventrolateral medulla (cVLM) which were reproducibly activated (Fig 1A-C). Analysis of these neurons revealed that they predominantly express the enzyme tyrosine hydroxylase (TH); we named these cells cVLMTH-neurons. As expected, capsaicin administration in Trpv1-null animals failed to activate these neurons (Fig. S1 A-B). Although, the cVLM has been previously reported to be stimulated by stressful stimuli[27,28], a role for this nuclei in pain control has not been examined. Intriguingly, despite using a unilateral stimulus, we found that cfos staining was bilateral, suggesting that the cVLM receives both ipsilateral and contralateral inputs (Fig 1D).

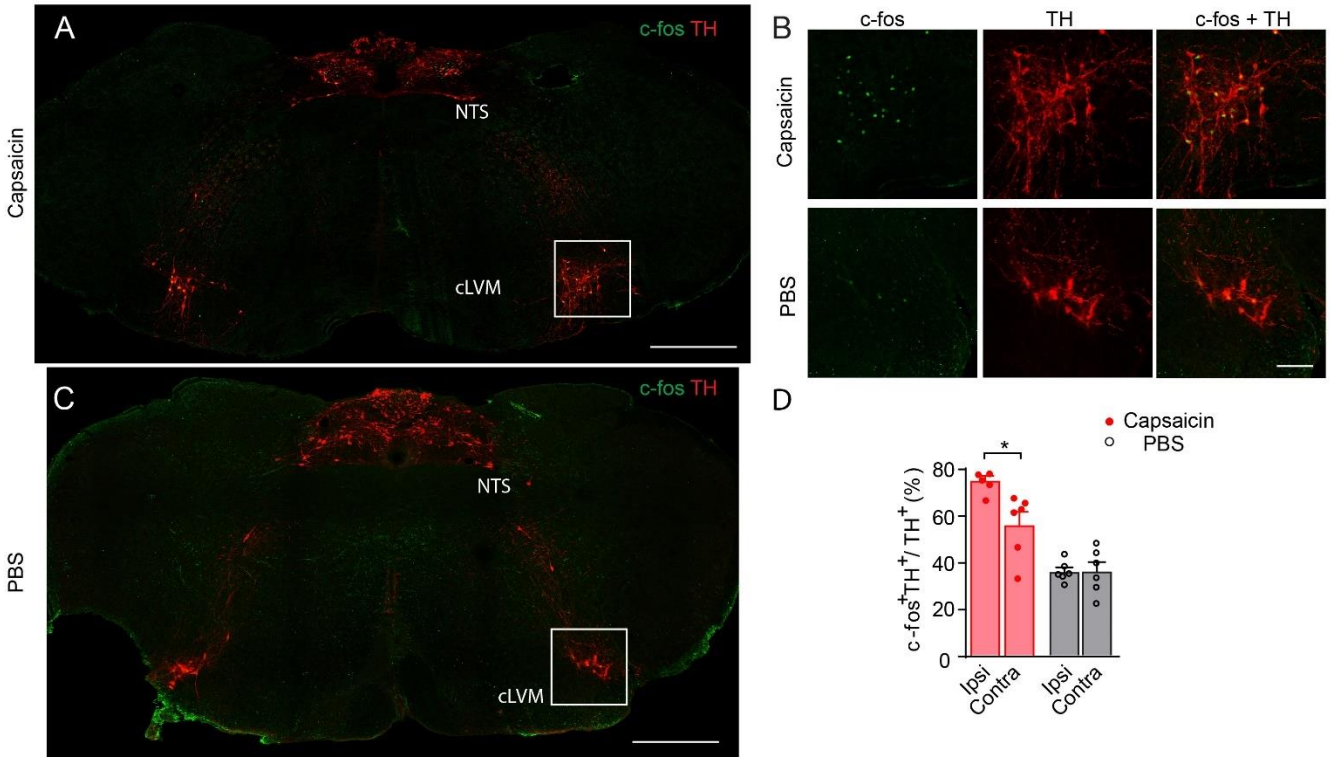

Fig 1. The cVLMTH, a brainstem nucleus activated by capsaicin.

A-C. Immunostaining for cfos in the caudal medulla of mice injected into the hind-paw unilaterally with capsaicin (A) or with saline (C) revealed that nociceptive stimulation increased numbers of TH^{+} neurons positive for cfos in the cVLM. B. Magnified view (see boxed area in A and C) of the cVLM showed that almost all TH-labeled neurons were cfos-positive after administration of capsaicin and few TH-neurons were cfos-labeled after saline treatment ($p=<0.001$, n=6 mice). D. The increase in the percent of cfos^{+}TH^{+} to TH^{+} neurons was more in the ipsilateral cVLM compared to contralateral side $p<0.010$, n=6 mice, Student T-test, data represent means $\pm$ SEM (Capsaicin ipsilateral 341/452, Capsaicin contralateral 219/404, PBS ipsilateral 154/440, PBS contralateral 147/371). Scale bars: 500 µm for coronal sections and 50 µm for magnified field images.

Since cfos-expression is a technique which does not allow real-time analysis of the kinetics of neural activation and to understand more about the types of stimuli which can activate cVLMTH-neurons, we turned to *in vivo* fiber photometry to probe calcium responses in these cells. Using TH-Cre mice together with stereotaxic injection of an AAV9-CAG-flex-GCaMP6s virus into the cVLM we could monitor cellular activity of cVLMTH-neurons (Fig 2A). We hypothesized that since these neurons are activated by capsaicin, they might also be activated by other noxious stimuli. Therefore, we challenged animals with several noxious in addition to innocuous stimuli. Consistent with our hypothesis, we observed increased intracellular calcium in cVLMTH-neurons upon injection of capsaicin, and challenge with noxious heat, and noxious mechanical pinch (Fig 2B-H). Calcium influx sharply increased when hot plate temperatures started to reach the noxious heat threshold of mice (~ 43-47°C; Fig 2E) and declined as temperature decreased. Importantly mild noxious and innocuous stimulation elicited minimal changes in calcium suggesting that these neurons are largely activated by strong noxious stimuli (Fig 2I and S2).

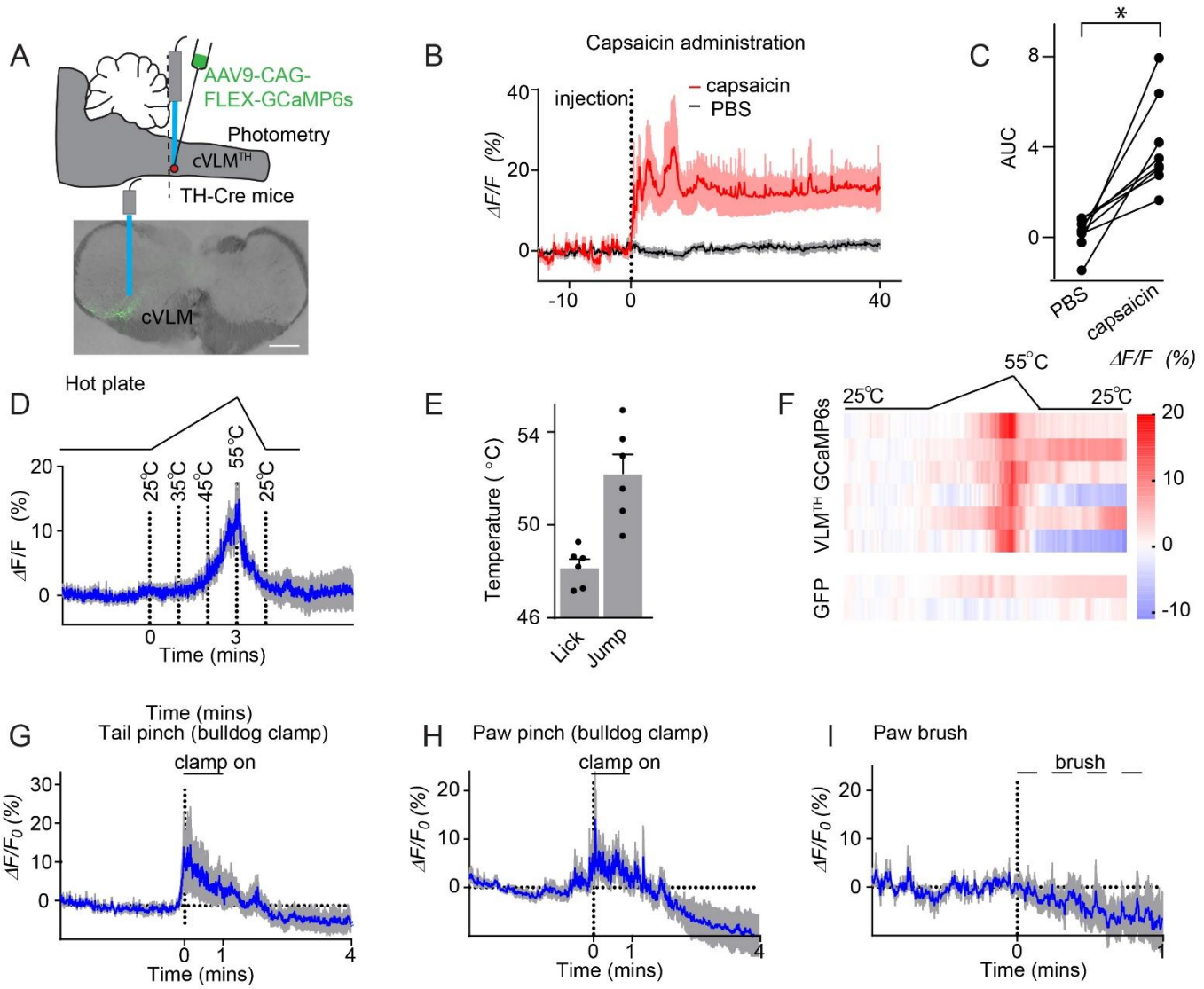

Fig 2. cVLMTH-neurons are activated by noxious stimuli.

A. Schematic of the procedures used to probe intracellular calcium responses of cVLMTH-neurons and a representative image (approx. position shown by dotted line) of GCaMP6s expression (lower panel). B. Averaged *in vivo* fiber photometry results from cVLMTH-neurons upon stimulation with capsaicin (red; injected into hind-paw) and saline (grey), n=8 mice, data are represented as mean results (red) ± SEM (shadow). C. Area under the curve (AUC) quantification showed that capsaicin treatment significantly increased calcium responses; p=0.0307, n=8 mice, Student paired T-test, data represent means ± SEM. D. Responses to heat challenge on a hot plate show intracellular calcium increased in cVLMTH-neurons in the noxious temperature range, n=6 mice. Hot plate

temperature linearly increased from 25°C to 55°C in 3 min. E. Nociceptive behavioral reaction coincided with increased calcium levels. F. Heatmap traces from 6 individual animals to heat challenge compared to those observed in GFP-expressing control animals (lower two traces). G-I. Calcium responses to bulldog pinch to the tail and hind-paw, and the fine brush stimulation of hind-paw respectively, averaged responses (blue) ± SEM (grey) n=6 mice.

Activation of cVLMTH- neurons triggers suppression of nociceptive responses

Our photometry experiments uncovered that cVLMTH-neurons are sensors of noxious insults, suggesting that the cVLM might be involved in a pain pathway. To investigate how they might participate in pain signaling, we examined the behavioral consequences of VLMTH-neuronal stimulation. For these experiments we engineered mice to express in cVLMTH-neurons designer receptors exclusively activated by designer drugs (DREADD) by injection of AAV coding for Cre-dependent Gq-coupled hMD3Dq (DREADDq) unilaterally into the cVLM of TH-CreER mice (Fig 3A-D). This chemogenetic approach should result in increased cfos staining of cVLMTH-neurons. Fig 3EF shows that, upon activation with CNO, there was a marked increase in numbers of cfos positive TH-neurons. We anticipated that if cVLMTH-neurons are part of an ascending nociceptive pathway, like neurons in the PBN[12-17], then their activation might elicit increased reactions to painful stimuli. Surprisingly, the activation of cVLMTH-neurons, instead of increasing sensitivity to noxious stimuli, evoked a profound suppression of responses to heat in Hargreaves tests (Fig 3G and see S3AB for controls), suggesting that, instead of being in an ascending pathway, cVLMTH-cells may be part of a nociceptive modulatory system. Additionally, unexpectedly for an ascending pathway, although we performed unilateral cVLM-stimulation, decreased sensitivity was induced in both hind paws (diffuse inhibition). This result also is indicative of a pain modulatory system. By contrast, chemogenetic activation of cVLMTH-neurons had no effects on behavioral responses to itch, cooling, and mechanical stimulation (including pinch) and additionally did not change core-body temperature and motor coordination (Fig S4A-F).

A corollary of chemogenetic activation of cVLMTH-neurons triggering decreased sensitivity to heat is that their inhibition, if they are tonically active in basal conditions, might elicit increased sensitivity. Indeed, DREADDi manipulation (Fig. 3H) reduced diffusely the

latency of withdrawal responses in Hargreaves assays suggesting that they normally provide inhibitory tone in naïve conditions (Fig 3I and S3CD). Similar to chemogenetic inhibition, ablation of cVLMTH-neurons, produced increased sensitivity to thermal challenge (Fig 3J). Like for chemogenetic activation, altered Hargreaves responses were the only sensory modality where we detected changed responses to chemogenetic inhibition (Fig S5A-F).

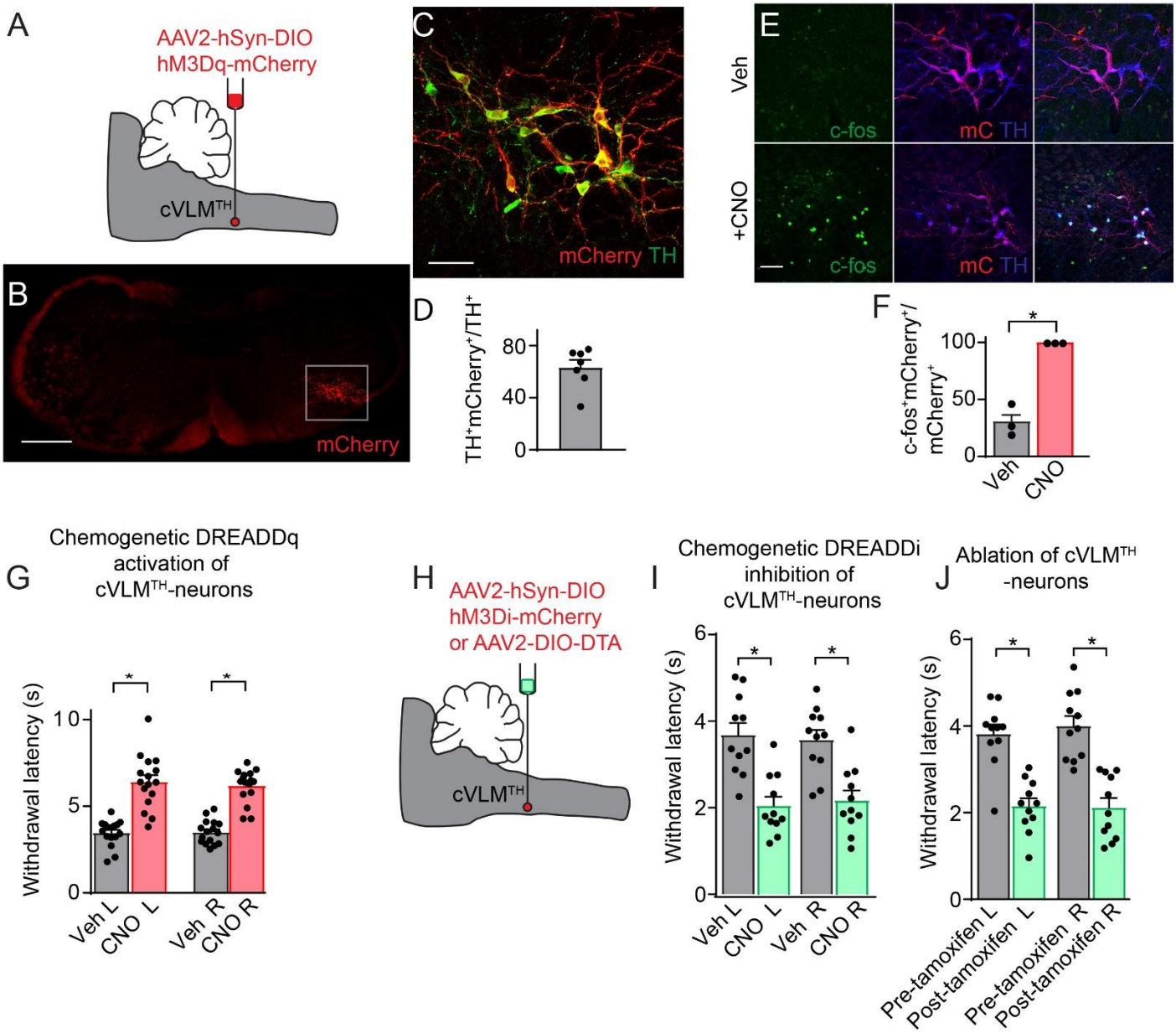

Fig 3. VLMTH-neurons potently control nociceptive behavioral responses.

A Schematic of the strategy employed to chemogenetically stimulate cVLMTH-neurons. B. Representative image showing the neurons expressing DREADDq-mCherry in the cVLM. C. Magnified view (boxed area in B) displaying that all mCherry expressing neurons are TH-positive. D. Quantification of the numbers of TH-neurons expressing mCherry, n=7 mice, data represent means ± SEM (mCherry$^+$TH$^+$/TH$^+$=177/281). E. Upon addition of CNO (lower panels), DREADDq stimulation led to cfos expression in TH$^+$-immunostained neurons. F. Quantification of the percentage of TH-neurons expressing cfos (Veh, cfos$^+$mCherry/mCherry$^+$=21/75, CNO, cfos$^+$mCherry/mCherry$^+$= 83/83). G. Withdrawal latencies were significantly increased, in Hargreaves tests, for mice where CNO was used to stimulate DREADDq in cVLMTH-neurons compared to saline injected mice (L and R indicate left and right hind-paw respectively), n=16, $p<0.001$, Student T-test. H. Schematic of the strategy employed to chemogenetically inhibit cVLMTH-neurons. I. Chemogenetic inhibition with DREADDi caused a significant shortening of withdrawal latencies compared to saline controls, n=11, $p<0.001$, Student T-test. J. Diphtheria toxin subunit A was expressed, after tamoxifen induction, in cVLM TH-neurons of TH-CreER mice. Ablation of cVLMTH-neurons caused a significant shortening of withdrawal latencies compared to saline controls, n=11, $p<0.001$, Student T-test.

While chemogenetics is a powerful technique to probe the function of neuronal ensembles, it has the disadvantage that it lacks temporal precision. Therefore, we employed optogenetics to more exactly examine the time course of cVLM induced changes in behavioral responses and the time required, after cessation of stimulation, for deactivation (Fig 4A). Similar to chemogenetic stimulation, these experiments revealed that optogenetic activation was effective at reducing sensitivity to noxious heat (Fig 4B). Interestingly results from this experiment showed that minutes after optogenetic stimulation had ended, there was still suppression of responses to noxious heat showing that cVLMTH-neurons activate a slowly desensitizing inhibitory circuit (Fig 4C). Together these results establish that, in an apparent feed-forward inhibitory circuit,

noxious stimuli activate cVLMTH-neurons which can in turn drive a specific and diffuse antinociceptive circuit.

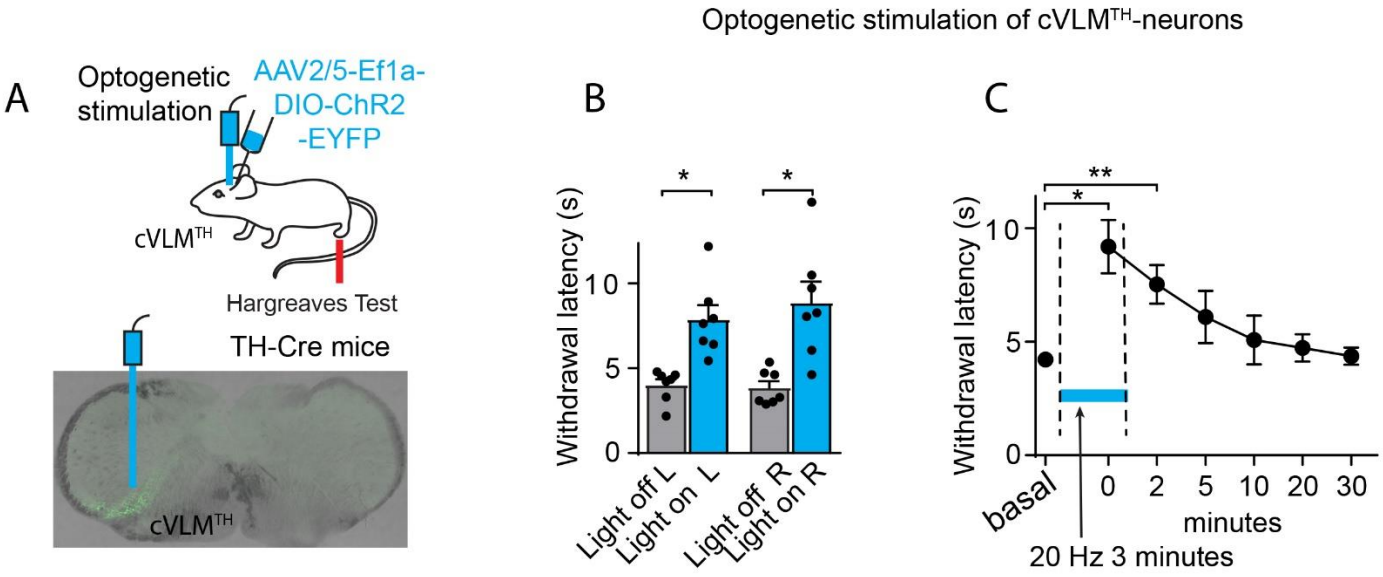

Fig 4. Optogenetic stimulation of cVLMTH triggers extended suppression of nociceptive responses.

A. Schematic of the strategy used to stimulate cVLMTH-neurons and representative image of ChR2 expression in the cVLM. B. Optogenetic stimulation caused a significant increase in withdrawal latencies in Hargreaves assays, compared to baseline, n=7, $p<0.05$ for L hind-paw and $p<0.01$ for R hind-paw, Student T-test, data represent means $\pm$ SEM. C. Time-course for activation and deactivation of attenuated responses to heat challenge (Hargreaves test) following optogenetic stimulation; testing was performed prior to, during (blue line), and after optogenetic stimulation. There was a significant difference in withdrawal responses compared to baseline during stimulation and at 2 min after the end of optogenetic stimulation, $p=0.025$ and $p=0.021$ respectively, n=7, Dunnett's tests following One-Way ANOVA.

cVLMTH-neurons are connected to a descending locus coeruleus spinal cord pathway

To broaden our understanding of the potential mechanisms by which the cVLMTH-ensemble triggers antinociception we investigated the downstream synaptic substrates of these cells. The approach we used was to inject Cre-dependent AAVs expressing mCherry and

synaptobrevin-GFP into the cVLM of TH-Cre mice to identify nerve fibers and their synapses respectively (Fig 5A).

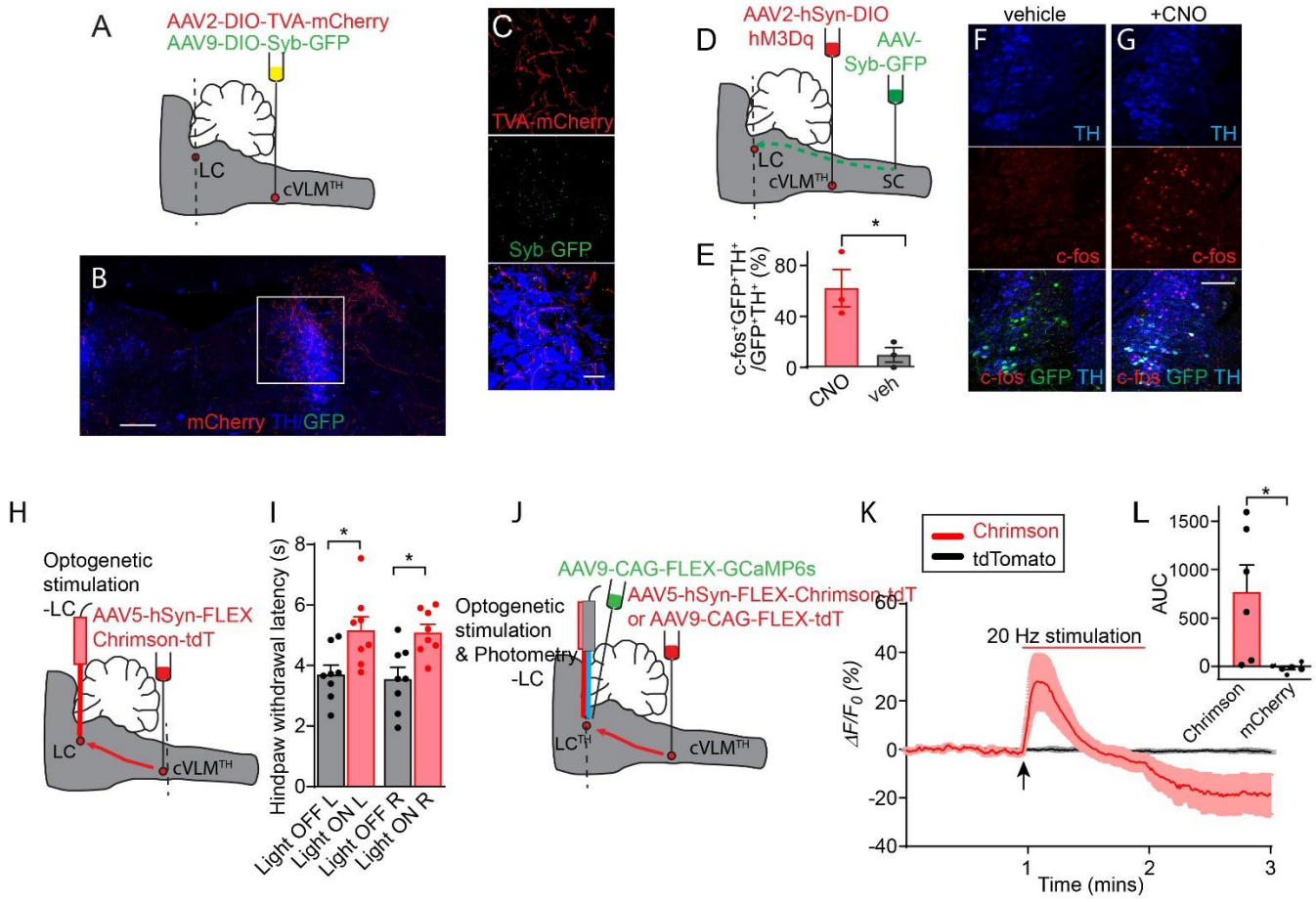

Fig 5. A descending antinociceptive cVLM-LC-spinal cord circuit.

A. Scheme showing the procedure used to identify synaptic partners of cVLMTH-neurons. B. Representative image of a section of the hindbrain (approx. position shown by dotted line A.) showing labeled fibers (red) and synaptic boutons (green) of cVLMTH-neurons. C. Magnified view of boxed area (in B). D. Strategy employed to stimulate cVLMTH-neurons and to label LC neurons projecting to the SC. E. Quantification of numbers of LC neurons projecting to the SC (GFP^{+}TH^{+}) which were cfos positive (cfos^{+}GFP^{+}TH^{+}) revealed a significant increase upon DREADDq stimulation (CNO) compared to saline control, n=3 mice, p=0.029, Student T-test, data represent means ± SEM (CNO, cfos^{+}GFP^{+}TH^{+}/GFP^{+}TH^{+} = 32/65, Veh, cfos^{+}GFP^{+}TH^{+}/GFP^{+}TH^{+}=3/30). F-G. Representative images of LC sections (approx. position shown by dotted line (D.) for mice administered vehicle (F.) or CNO (G.) showed an increase in cfos (red) labeling

in spinal cord projecting neurons following chemogenetic activation of cVLMTH-neurons. H. Diagram of the approach used to optogenetically activate LC-projecting cVLMTH-neuronal fibers. I. Optogenetic stimulation caused a significant increase in withdrawal latencies in left (L) and right (R) hind-paws, in Hargreaves assays, compared to baseline, n = 8, p=0.0097 for left and 0.0196 for right hind-paws, paired Student T-test, data represent means ± SEM. J. Diagram of the approach used to optogenetically activate LC-projecting cVLMTH-neuronal fibers in conjunction with record calcium responses in LC-neurons. K. Measurement of calcium responses in LC-neurons using *in vivo* fiber photometry showed that stimulation of LC projecting cVLMTH-neuronal fibers rapidly increases intracellular calcium in LC neurons, data are represented as mean results (red or black line) ± SEM (pink or grey). L. Quantification of area under the curve (AUC) responses show that activation of Chrimson expressing fibers produces significantly more responses compared to tdTomato-expressing fibers, n=6, p=0.0168 Student t-test, data represent means ± SEM. Scale bars: 500 µm in B, H and J; 50 µm in C, 100 µm in F and G.

This approach revealed that cVLMTH-neurons terminate in several brain nuclei (Fig 5BC and S6A-G). In particular, we found strong labeling of the locus coeruleus (LC) (Fig S7A-G). In addition to the LC, as reported previously, we uncovered terminals in the periaqueductal grey (PAG), the paraventricular hypothalamus (PVN), paraventricular thalamus (PVT), and the bed nucleus of the stria terminalis (BNST)[29,30](Fig S6). The LC is a brain-nucleus well-known to mediate analgesia through descending SC projections[18,19,31], suggesting that it could be a partner that could account for the downstream inhibitory effects of the cVLM. To determine whether the LC is functionally engaged by the cVLM we used three complementary experimental approaches. First, using cfos-expression as a metric for cell-activation, we investigated whether activation of cVLMTH- neurons is sufficient to excite LC-neurons (Fig 5D). For these experiments, we again chemogenetically activated cVLMTH- neurons in conjunction with labeling LC-SC projecting neurons (by intra-spinal injection of GFP-expressing AAV in the SC) and determined numbers of spinally projecting LC-neurons positive for cfos. Using this approach, we observed robust activation of LC-SC neurons consistent with activation of the LC by the cVLM (Fig 5E-G). Second, we examined whether activation of terminals of cVLMTH-

neurons projecting to the LC can modulate nociceptive responses (Fig 5H). Specifically, we injected an AAV (Cre-dependent Chrimson) into the cVLM of TH-Cre mice and optogenetically stimulated cVLMTH -nerve terminals in the LC. Fig 5I shows that the activation of cVLMTH-fibers increased withdrawal latencies corroborating that the LC is an important route for cVLM-mediated inhibition of heat responses. Thirdly, we assessed whether calcium responses in LC-neurons can be evoked by the activation of the cVLMTH-ensemble. The strategy we used was to optogenetically stimulate cVLM-terminals together with imaging of LC-cells (Fig 5K). Results from these experiments establish that the activation of LC-neurons is tightly connected with stimulation of the cVLMTH-ensemble (Fig 5LM).

Lastly, we wanted to determine if release of NA by spinally projecting LC-neurons (LC-neurons are noradrenergic) is required for cVLMTH-mediated inhibition of withdrawal responses to heat. For these experiments we chemogenetically activated cVLMTH- neurons and examined whether the injection of the α2-adrenergic receptor antagonist yohimbine could block the cVLMTH -chemogenetic-induced reduction in heat sensitivity (Fig 6A). Exactly as expected for a descending noradrenergic pathway[19], this treatment blocked cVLM chemogenetic-induced attenuation of responses (Fig 6B) suggesting that a major descending pathway of the cVLM is via the LC and requires the neurotransmitter NA. If NA is a transmitter that is required for cVLM induced antinociception, then cVLM-induced pronociception should be reduced by administration of an α2- adrenergic receptor agonist. Exactly as predicted, clonidine treatment almost completely alleviated chemogenetic (DREADDi) mediated sensitization to heat (Fig 6D). In contrast, pharmacological intervention of serotonin signaling [32,33] was ineffective at relieving cVLM-induced pronocicieption (Fig 6EF). Together, these results suggest that the LC is an important route and the transmitter NA is critical for cVLM-induced modulation of nociceptive responses.

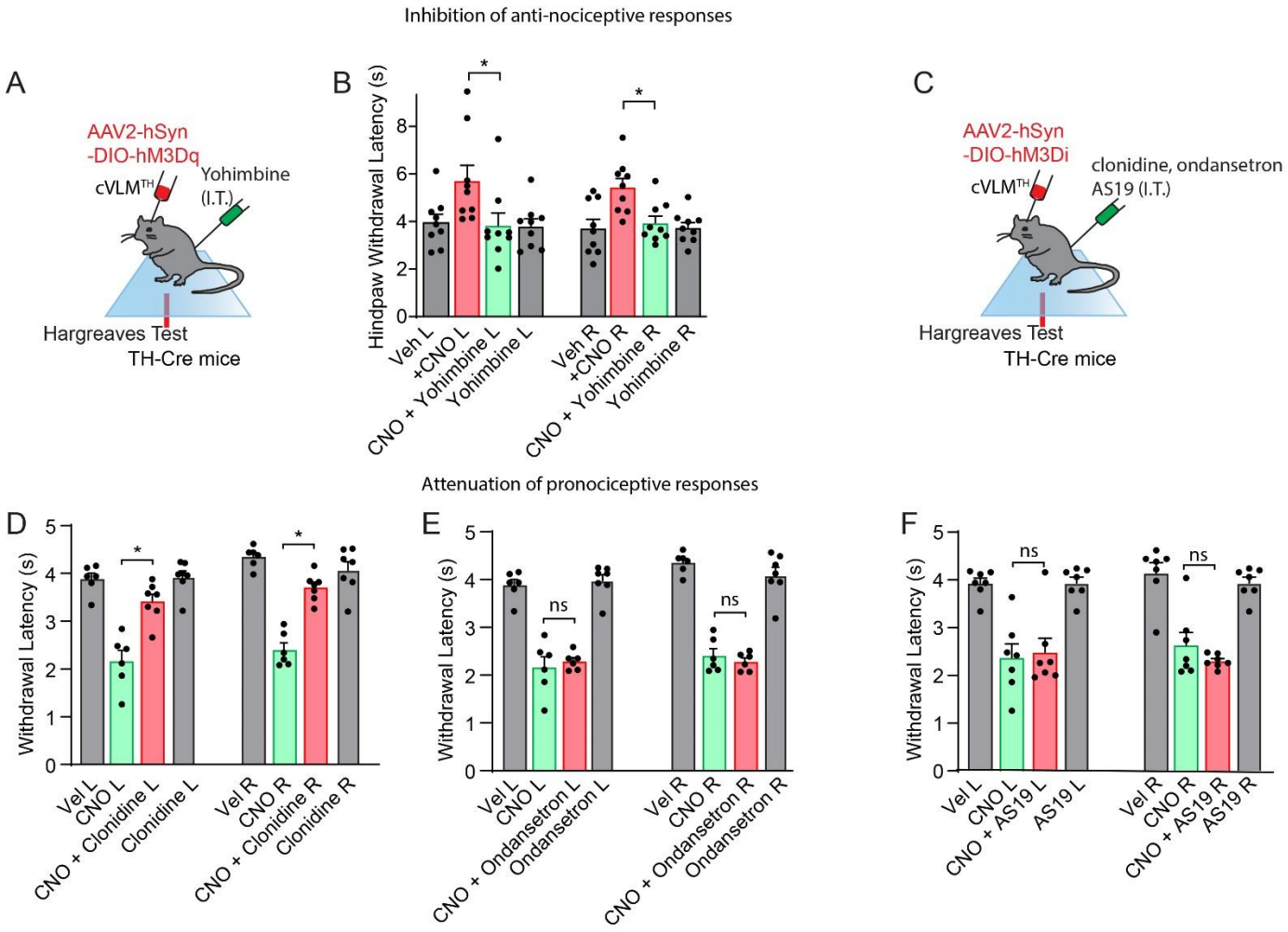

Fig 6. Antinociceptive and pronociceptive responses induced by cVLMTH-neurons are disrupted by spinal cord administration of α2-adrenergic receptor antagonist and agonist respectively.

A. Experimental paradigm used to examine the influence of spinal cord noradrenalin on cVLMTH-neuron induced antinociceptive effects. B. Chemogenetic activation (DREADDq) of cVLMTH-neuron induces increased withdrawal latencies in Hargreaves test which were significantly attenuated by intrathecal administration of yohimbine, n=9, p=0.050 for L and 0.018 for R hind-paws respectively, Student T-test, data represent means ± SEM. C. Chemogenetic inhibition (DREADDi) of cVLMTH-neurons produced pronoception likely through adrenergic modulation. D. Intrathecal injection of the α2-adrenergic agonist, clonidine, reversed the CNO-induced sensitization of hind-paw responses measured with the Hargreaves tests, n = 7, p <0.001, for both L and R hind-paws, paired Student T-test, data

represent means ± SEM. E. By contrast, the serotonin 5-hydroytryptamine type 3 (5-HT3) receptor antagonist ondansetron (suggested to be responsible, in part, for descending facilitation of pain from the RVM) had no effect on CNO-induced hyperalgesia, n=7, p=0.578 for L (left) and p=0.341 for R (right) hind-paws. F. Similarly, 5-hydroytryptamine type 7 (5-HT7) receptor agonist, AS19 (thought to be responsible, in part, for the descending inhibition of pain from the RVM) also did not affect CNO-induced hyperalgesia, n=7, p=0.858 for L and p=0.363 for R hind-paws, paired Student T-test, data represent means ± SEM.

The cVLM is required for counter-stimulus and glucoprivation induced analgesia.

Our results show that the cVLM-circuit produces a diffuse reduction in responses to heat through a feed-forward pathway which terminates in the spinal cord. The characteristics of this circuit are similar to those reported for several descending inhibitory pathways including DNIC whose cellular substrate and circuit have remained elusive for over 40 years[23,25,26,34]; DNIC can be stimulated by multiple noxious stimuli, uses NA, produces inhibition which is slow to dissipate, and whose supraspinal nuclei has been reported to located in the brainstem. What is the physiological roles of the cVLM-circuit? One possibility is that it is involved in state-dependent pain control processes like those proposed for DNIC[3,9,24,35] including counter-stimulus induced analgesia (pain inhibition of pain)[23].

To test the hypothesis that the cVLM might be involved in counter-stimulus induced analgesia, we performed three tests. First, we probed whether the activation of the cVLM-circuit is sufficient to alleviate thermal allodynia (a pain state). We injected CFA into a hind-paw of mice to produce inflammatory pain and tested whether chemogenetic activation of the cVLMTH-neurons could reverse the resulting increased thermal sensitivity. Responses in the injured foot, after cVLM-activation, were returned almost to baseline, demonstrating that cVLM-activation is sufficient to reverse thermal allodynia (Fig 7A). Second, we examined whether GCamp6-responses of cVLMTH-neurons to noxious challenge are reduced following administration of a counter-stimulus. We compared responses of cVLMTH-neurons to the same noxious heat stimuli (three 55 ºC ramps) before and then after administration of a painful counter-stimulus (injection of 10 µg capsaicin into a forepaw) (Fig 7BC). Naïve mice were first tested to determine their baseline responses to noxious heat stimuli. Next, these same mice were again tested (after a 1-

hour rest period) with the same 3 noxious heat stimuli after the administration of a counter-stimulus. Exactly as postulated for a feed-forward inhibitory loop, the counter-stimulus reduced the calcium responses to the heat challenge (second hot-plate challenges) (Fig 7DE, also see controls Fig S8). Also as expected for a pain inhibition of pain process, after administration of the counter stimulus mice exhibited delayed behavioral responses to the hot plate challenge relative to naïve mice (Fig S8B). Third, we examined whether cVLMTH-neurons are required for counter-stimulus induced analgesia. We developed a mouse model of counter-stimulus induced analgesia. In this model, the reactivity to heat was assessed in an injured paw (mild-burn) and then a counter stimulus delivered (capsaicin injection into a forepaw) and the assay repeated comparing the withdrawal responses before and after counter-stimulus administration. (Fig 7F). Using this model, we found that a counter-stimulus can produce analgesia in the injured hind-paw (Fig 7G). Next, we tested whether the chemogenetic inhibition of cVLMTH-neurons can attenuate counter-stimulus induced analgesia. We repeated our model but for these experiments we used mice where we could chemogenetically inhibit of cVLMTH- neurons (Fig 7H). Demonstrating that the cVLM is required for counter-stimulus induced analgesia, when the cVLMTH-neurons are inhibited, counter-stimulus induced analgesia was eliminated (Fig 7I). Together our results demonstrate that the cVLM-circuit is both required and sufficient for counter-stimulus induced analgesia.

We recently investigated the contribution of output from cVLMTH-neurons to the PVT in food-seeking and consumption behaviors (unpublished results; Beas et al, 2020 under Review Nature Communications). These studies showed that, as previously reported, the cVLM is activated during extreme glucose privation (glucoprivation)[27]. In addition to being involved in homeostatic feeding responses to glucoprivation, it has been reported that glucoprivation itself can induce analgesia[5]. Therefore, we wondered whether the cVLM might also be involved in this type of analgesic response. To test this prediction, we induced glucoprivation by administration of 2-deoxy-D-glucose (2DG) and examined whether the resulting antinociceptive responses could be attenuated by chemogenetic inhibition of cVLMTH-neurons. Indeed, exactly as anticipated, cVLMTH-neurons were required for this type of stressor induced analgesia (Fig 7JK).

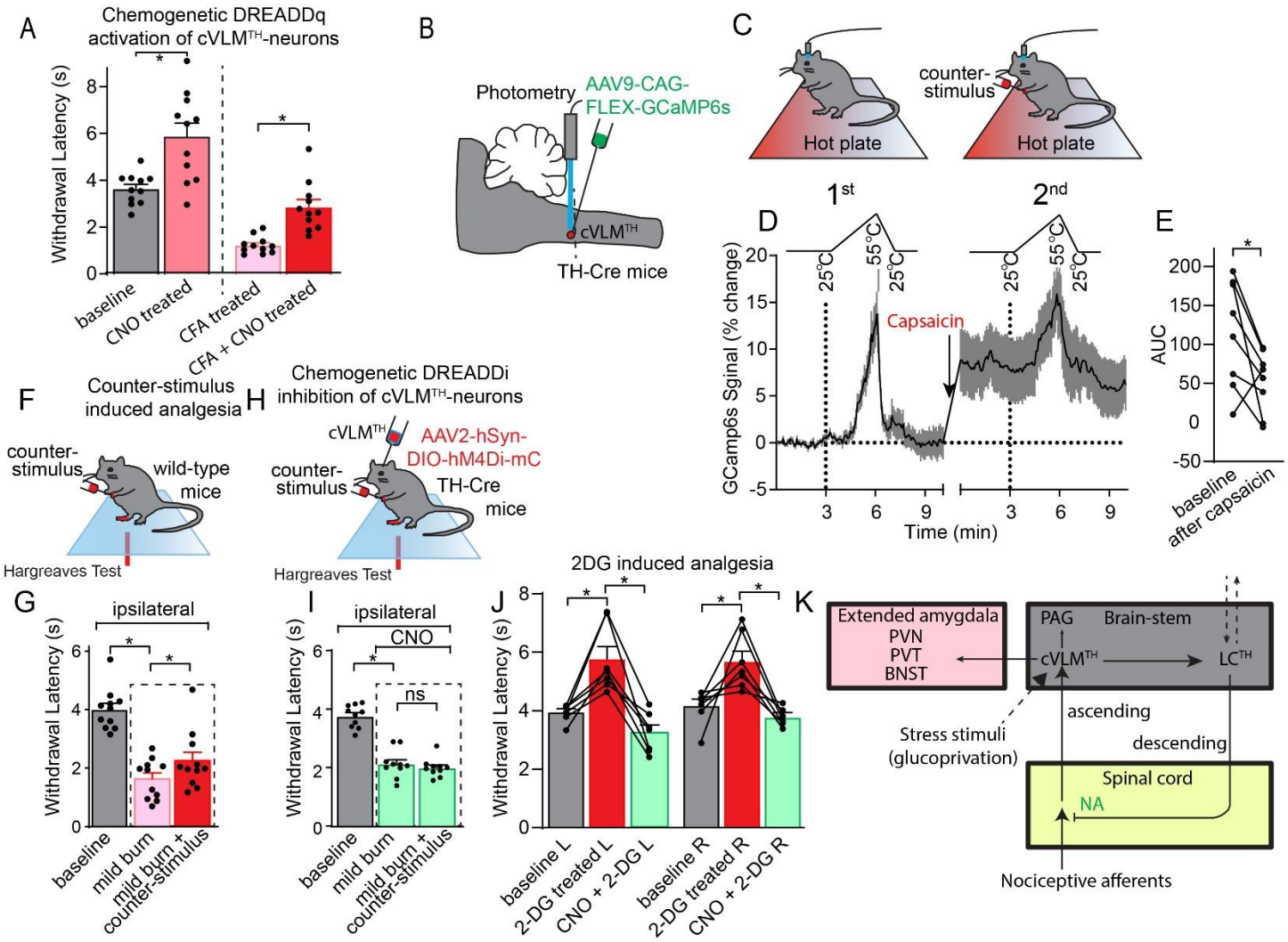

Fig 7. The cVLM-circuit is required and sufficient for counter-stimulus induced analgesia.

A Chemogenetic activation of cVLMTH-neurons significantly lengthens withdrawal latencies to heat stimulation after inflammation (complete Freuds Adjuvant (CFA)), n=11 mice, $p<0.001$ Student T-test, data represent means $\pm$ SEM. BC. Schematic of procedures used to record changes in intracellular calcium in cVLMTH-neurons and the experimental design used to examine the effects of counter-stimulation on responses to hot plate temperature ramps; mice were tested three times (1st) with 55 ºC ramps, mice were given a 1-hour rest and then injected with capsaicin (as indicated). Next, a further three heat ramps trials were performed (2nd). D. Averaged responses over trials before and after counter-stimulation showed that responses to individual ramps were diminished after capsaicin treatment, data

are represented as mean results (black line) ± SEM (grey). E. Quantification of area under the curve (AUC) for responses to heat ramps were significantly reduced after capsaicin treatment, n=8 mice, p=0.033 Student T-test, data represent means ± SEM. F. Scheme showing the experimental design for measurement of counter-stimulus induced analgesia; one hind-paw received a mild-burn (ipsilateral) and withdrawal latencies were determined using the Hargreaves test before and after capsaicin injection into a forepaw. G. Latencies for withdrawal of the ipsilateral paw were significantly reduced compared to baseline after mild burn and were significantly increased compared to mild-burn after administration of counter stimulus, n=11 mice, p=<0.0010.0001 and p=0.035 respectively, Student paired T-test, data represent means ± SEM. H. Diagram depicting the approach used to determine the effect of cVLMTH-circuit on counter-stimulus induced analgesia. I. Chemogenetic inhibition of cVLMTH-neurons prevented attenuation of counter-stimulation (capsaicin) induced analgesia of the ipsilateral paw, p=0.121, while mild-burn was significantly reduced compared to baseline p=<0.001, n=10 mice, Student T-test, data represent means ± SEM. J. Chemogenetic inhibition of cVLMTH-neurons prevented 2DG induced analgesia. Hargreaves withdrawal responses were significant longer after 2DG treatment compared to baseline, p=0.005 and p=0.023 for left (L) and right R paws respectively, and 2DG responses were significantly reduced compared to chemogenetic inhibition (CNO), p=0.001 and p=0.003 for L and R paws respectively, n=7 mice, Student T-test, data represent means ± SEM. K. Proposed model for feed-forward inhibition by the cVLM-circuit.

Discussion

The cVLM-circuit displays features of an inhibitory pathway like that responsible for DNIC, however it was shown previously that DNIC can attenuate both thermal and mechanical pain[25,26] and while the cVLM-circuit inhibits thermal responses, it does not alter mechanical nociception. Therefore, we propose that the cVLM-circuit may be part of the DNIC pathway which may include additional brainstem nuclei. The reason why only responses to heat are effected by the cVLM-circuit is unclear but thermal and mechanical nociceptive ascending pathways are known to be segregated[36-42]. In addition, there are multiple reports for ascending PbN[13], for descending PAG-RVM-SC[20,43], and for the descending corticospinal pathways[44] where behavioral effects are described to be modality specific. These studies, like ours, used artificial means to experimentally probe neural ensembles within discrete circuits and while these approaches are powerful, they are different from what occurs under normal physiological settings where likely multiple interconnected and coordinated ascending and descending pathways operate. Therefore, the output of the cVLM-circuit could be coordinated with other pathways to produce analgesia. Indeed, this explanation fits with studies showing that, to produce global control of pain, there is considerable interaction between the descending LC noradrenergic and the RVM serotonergic (inhibitory and faciliatory) systems[3,9,24,35].

Other stress stimuli activate the cVLM[27,28,45-47], suggesting that the cVLM may act as a coordinating center that integrates various inputs to ensure a well-organized, coherent and appropriate set of responses[48,49 50]. Supporting this concept, we found that glucoprivation induced analgesia requires cVLM activity. Other interoceptive and somatic stimuli that convey harmful circumstances (stressors) may likewise activate the cVLM producing diffuse analgesia as well as other responses that are ethologically useful for survival in adverse conditions.

In addition to the efferent connection of the cVLM with the LC, the cVLM has reciprocal connections with the PVN through which it could participate in modulation of the HPA-axis[28,46]. Furthermore, the cVLM probably relays signals to affective brain regions via connection with the PVT[27], and BNST[30]. In the future, it will be interesting to examine the potential functional contributions of these connections in the context of pain relative to different internal states as well as investigating the nature of the different afferent inputs into the cVLM.

Conditioned pain modulation (CPM), likely the human counterpart of DNIC, has been extensively studied in healthy and in chronic pain patients[51-54]. Intriguingly, CPM is diminished in pain states, NA-based therapies can alleviate symptoms in these conditions, and there is a prospective correlation between patients' ability to produce CPM and their chances for development of chronic pain[55-58]. Interestingly, the phenotype of mice in which cVLMTH-neurons are inhibited is similar to that seen in some forms of chronic pain[24], suggesting that the techniques we describe here could serve as a starting point to investigate signaling pathways involved in these diseases. Therefore, targeting the cVLM-pathway might provide a means to both investigate and treat pain including the pain found in chronic diseases.

Acknowledgments

We thank Alena Hoover, Erich Henry, and Caitlyn De Preter for their help, at the beginning of this project, in collecting preliminary data. This work was supported by the intramural research program of the National Institute of Dental and Craniofacial Research, National Institutes of Health, project ZIADE000721-20 (MAH).

Author contributions

X. G., and M.A.H. designed the experiments, analyzed data and wrote and edited the paper. X.G. performed experiments.

Competing interests

We declare no competing interests.

Methods

Animals: All experiments using mice followed NIH guidelines and were approved by the National Institute of Dental and Craniofacial Research ACUC. Mice were housed in small social groups (4-5 animals) in individually ventilated cages under 12-hour light/dark cycles and fed *ad libitum*. Animals of both genders with the age of 7-12 weeks were used in experiments. C57Bl/6N wild-type mice were purchased from Envigo (Indianapolis, IN). TH-IRES-CreER mice (The Jackson Laboratory, stock #00852) and TH-IRES-Cre mice (European Mouse Mutant Archive; stock #: EM:00254; backcrossed 5 generations with C57Bl/6NJ mice) were bred in house. Animals were randomly allocated to the different experimental conditions reported in this study. Genotyping of offspring from all breeding steps was performed with genomic DNA isolated from tail snips and Cre primer pairs.

Viral vectors: AAV2/5-Ef1a-DIO hChR2(E123T/T159C)-EYFP, AAV9-CAG-FLEX-GCaMP6s-WPRE-SV40 and AAV9-hSyn-eGFP were obtained from the Vector Core of the University of Pennsylvania. AAV9-CAG-FLEX-tdTomato, AAV2-mCherry-FLEX-dtA, AAV9-hSyn-DIO-mCherry-2A-SybGFP, AAV2-hSyn-DIO-hM4Di-mCherry and AAV2-Syn-DIO-GFP were produced by the Vector Core of the University of North Carolina. AAV5-Syn-FLEX-

ChrimsonR-tdTomato (Addgene plasmid # 62723) and AAV2-hSyn-DIO-hM3D(Gq)-mCherry (#44361-AAV2) were produced by Addgene. AAV2(retro)-CAG-iCre (Addgene plasmid # 81070) was produced by Vector Biolabs. All viral vectors were stored in aliquots at −80°C until use.

Drugs: Clozapine N-oxide (CNO) (Abcam, catalog#ab141704) was used at a 10 mg/Kg dose when used in combination with the excitatory DREADDq and at 0.75 mg/Kg with inhibitory DREADDi virus. Capsaicin (Sigma, catalog #M2028) was dissolved in alcohol at 100mg/ml and was diluted to 1 mg/ml working solution with PBS containing 5% Tween-20. Yohimbine hydrochloride was dissolved in DMSO and diluted to 1mg/ml working solution with PBS. AS19 (Tocris, catalog#1968) was dissolved in DMSO and diluted with PBS. Ondansetron hydrochloride (Tocris, catalog #2891, 10 µg), clonidine hydrochloride (Tocris, catalog #0690, 1nmol), AS19 (Tocris catalog #1968, 10 µg) were prepared with sterile PBS. The Complete Freund's Adjuvant (CFA, Sigma, catalog#F5881,10 ul, subcutaneously injection) was used to induce inflammatory pain. 2-Deoxy-D-glucose (Tocris, catalog#4515, 500 mg/kg) was injected intraperitoneally into the mouse 30 minutes after CNO administration and 30 minutes before Hargreaves tests.

Antibodies: Primary antibodies: anti-cFos (1:500, goat polyclonal, Santa Cruz catalog #sc-52-G; 1:50, rabbit monoclonal, Cell Signaling, catalog # 2250); and anti-TH (1:1000, Emd millipore, rabbit polyclonal, catalog #AB152 or 1:1000 mouse monoclonal, catalog #MAB5280). Fluorophore-conjugated secondary antibodies were purchased from ThermoFisher Scientific. Antibodies were diluted in PBS with 10% NGS and PBST.

Stereotaxic surgery: All stereotaxic surgeries were conducted as described in our animal study protocol. Mice were anesthetized with a Ketamine/Xylazine solution (100mg/10mg in PBS) and a stereotaxic device (Stoelting, USA) was used for viral injections at the following stereotaxic coordinates: cLVM, -2.50 mm from Lambda, ±1.40 mm lateral from midline, and -5.30 mm vertical from cortical surface. LC, -5.50 mm from Bregma, 0.95 mm lateral from midline, and -3.50 mm vertical from cortical surface. AAVs were injected with an oil hydraulic micromanipulator (Narishige). AAVs were injected at a total volume of 0.1 µl in the cVLM. All

other AAVs were injected at approximately 0.2-0.3 µl. Following stereotaxic injections, AAVs were allowed 2-3 weeks for maximal expression. Optical fibers with diameters of 200 µm (0.48 NA) and 400 µm (0.66 NA), were used for optogenetics and fiber photometry experiments, respectively (Doric Lenses). These fibers were implanted over the cLVM or LC immediately after viral injections and cemented using C&B Metabond Quick Adhesive Cement System (Parkell, Inc.). Mice received subcutaneous injections with Ketoprofen (5 mg/kg) for analgesia and anti-inflammatory purposes pre- and post-operatively and were allowed to recover on a heating pad where they were constantly monitored.

Histology: Mice were euthanized with CO2 and subsequently subjected to transcardial perfusion with PBS and then with paraformaldehyde (PFA; 4% in PBS). Brains were then postfixed in 4% PFA at 4 °C overnight, and cryoprotected using a 30% PBS-buffered sucrose solution for ~24-36 h. Coronal brain sections (40 µm) were acquired using a cyrostat (CM1860, Leica). For immunostainings, brain sections were blocked in 10% normal goat serum (NGS) in PBST (0.3% Triton X-100 in PBS) for 1 hr at RT, followed by incubation with primary antibodies in 10% NGS-PBST for 24-48 hrs at 4 °C. Sections were then washed with PBST (3 × 15 min) and incubated with fluorescent secondary antibodies at RT for 1 h in 10% PBST. Sections were washed in PBS (3 × 15 min), mounted onto glass slides and cover-slipped with Fluoromount-G (SouthernBiotech, catalog #0100-01). Images were taken using a Nikon C2+ confocal microscope. Image analysis and cell counting were performed using ImageJ software by a blinded experimenter (Fiji, version 2017 May 30).

Bulk Ca2+ and Fiber photometry: Fiber photometry procedures and calcium measurements were performed by following methods previously described[59]. Mice were first allowed to adapt to the experimental chambers and attached fiber patchcord for 60 min prior to each testing session. The fiber photometry system (Doric Lenses) was used to record fluorescence signals. The system is integrated with two continuous sinusoidally modulated LED (DC4100, ThorLabs) at 473 nm (211 Hz) and 405 nm (531 Hz) that served as light source to excite GCaMP6s and an isosbestic autofluorescence signal respectively. Fluorescence signals were collected by the same fiber implant that was coupled to a 400 µm optical patch-cord (0.48 NA) and focused onto two separate photoreceivers (2151, Newport Corporation). The RZ5P acquisition system (Tucker-

Davis Technologies; TDT), equipped with a real-time signal processor controlled the LEDs and also independently demodulated the fluorescence brightness due to 473 nm and 405 nm excitation. The LED intensity (ranging 10–15 μW) at the interface between the fiber tip and the animal was constant throughout the session. All photometry experiments were performed in behavioral chambers (Coulbourn Instruments), square enclosure on hot plate (IITC Life Science) or mouse enclosures for Plantar Test Instrument (Ugo Basile). For ΔF/F analysis, a least-squares linear fit to the 405 nm signal to align it to the 470 nm signal was first applied. The resulting fitted 405 nm signal was then used to normalize the 473 nm as follows: ΔF/F = (473 nm signal − fitted 405 nm signal)/fitted 405 nm signal. Lastly, changes in fluorescence after stimulation or after capsaicin injection were determined by the area under the ΔF/F curve, before and after stimulus.

Optogenetics: TH-IRES-Cre mice injected with either Cre-dependent ChR2 or Cre-dependent GFP (control) in the cVLM and an optical fiber placed above cLVM were behaviorally tested three weeks later. Mice were tethered with an optical patch cord and placed in the perspex enclosure (10 cm x 10 cm x 15 cm) with free movements. After the habituation for 60 mins, Hargreaves test were performed to measure the baseline of hind-paw withdrawal latency. Then, mice received light stimulation with a blue LED light (470 nm, Thorlab M470F1) at a frequency of 20 Hz (10 ms width) for 2 min. Hargreaves tests were carried out to measure the hind-paw withdrawal latency during the stimulation and at 2 min, 5 min, 10 min, 20 min and 30 min after cessation of stimulation. For optical activation with Chrimson, a 561 nm laser (Opto Engine LLC, 561-50mW) was used to generate light stimulation at a frequency of 20 Hz (10 ms width) for 2 min during which Hargeaves tests were performed.

Mouse behavioral measurements

All behavioral experiments were conducted during the light cycle at ambient temperature (~23 ˚C).

Plantar Test (Hargreaves Test): Mice were habituated to the testing enclosures (Ugo Basile, Gemonio, Italy) for 60 min. Habituation was repeated for 2 days. On testing day, after the mice were acclimatized for 60 min in the testing enclosure, a radiant heat beam was applied to the center of the hind paw and reaction time between the start of the heat stimuli and lifting the hind-

paw were recorded as the hind-paw withdrawal latency. A cut-off time of 15 s was used to prevent tissue damage. Consecutive tests of the same paw were separated by at least 3 minutes. The test was repeated for 5 trials for both left and right hind-paws. The averages of the withdrawal latencies were calculated. Mild burn was achieved by placing the hind paw, while mice were deeply anesthetized, in a water bath at 55°C for 15 s.

Cold test: Cold responses were tested as described previously [60]. Briefly, a dry ice pellet was applied below the hind paw of a mouse sitting on a glass surface and time to withdrawal was measured. Withdrawal was tested 5 times for each hind paw, consecutive tests of the same paw were separated by at least 3 minutes.

Itch test: Behavioral assessment of scratching behavior was conducted as described previously [38]. Briefly, mice were injected subcutaneously into the nape of the neck with chloroquine. Compounds were diluted in PBS. Scratching behavior was recorded for 30 minutes and is presented in numbers of bouts observed in 30 minutes. One bout was defined as scratching behavior towards the injection site between lifting the hind leg from the ground and either putting it back on the ground or guarding the paw with the mouth. Injection volume was always 10 µl.

Von Frey test: Mechanical sensitivity thresholds were assessed using calibrated von Frey filaments employing the simplified up-down method. Animals were acclimatized in a plastic cage with a wire mesh floor for 1 hour and then tested with von Frey filaments with logarithmically incremental stiffness (starting with 0.4g). Each filament was applied for 5 sec, and the presence or absence of a withdrawal response was noted. The filament with the next incremental stiffness was then applied, depending on the response to the previous filament, and this was continued until there had been 6 positive responses. The filaments were applied to the glabrous skin on the hind paw, and a positive response was recorded when there was lifting or flinching of the paw. The force required for 50% withdrawal was determined by the up-down method.

Rota-rod test: Motor coordination was tested by measuring the performance on an accelerating rota-rod (IITC) with the rod programmed to accelerate from 4 to 40 rpm over 5 mins. During the experimental testing session, the mice were allowed two trial runs followed by 4 test runs and the average of the maximum rpm tolerated was recorded. For each mouse, the ratio of maximum

rpm during CNO/vehicle treatment over pre-operative maximum rpm was determined. Each mouse performed the task 3 times and the rod speed at failure was averaged.

Intrathecal injections: We used the method described previously[61] to administer drugs into the spinal cord. Mice were anesthetized with isoflurane. The caudal paralumbar region, just cranial to the iliac crests, was securely held by the thumb and middle fingers of the left hand, and the index finger was placed on the tip of sixth lumbar (L6) spinous process, the highest point of the vertebral column. All intrathecal injections were delivered in a total volume of 10 µl. The needle was inserted into the fifth intervertebral space (L5–L6) causing a sudden lateral movement of the tail. The needle was held in position for 10 s and removed slowly to avoid outflow.

Quantification and statistical analysis: Prism 7.0 (GraphPad Software, La Jolla, CA) was used for statistical analyses. Differences between mean values were analyzed using paired two-tailed Student's t-test Differences were considered significant for $*P < 0.05$. Exact p-values, definition and number of replicates as well as definitions of center and dispersion are given in the respective Fig legend. No statistical method was employed to predetermine sample sizes. The sample sizes used in our experiments were similar to those generally used in the field.

References

1. Basbaum, A.I., Bautista, D.M., Scherrer, G. & Julius, D. Cellular and molecular mechanisms of pain. *Cell* **139**, 267-284 (2009).
2. Beecher, H.K. Pain in Men Wounded in Battle. *Ann Surg* **123**, 96-105 (1946).
3. Fields, H.L. & Heinricher, M.M. Brainstem modulation of nociceptor-driven withdrawal reflexes. *Ann N Y Acad Sci* **563**, 34-44 (1989).
4. Alhadeff, A.L.*, et al.* A Neural Circuit for the Suppression of Pain by a Competing Need State. *Cell* **173**, 140-152 e115 (2018).
5. Bodnar, R.J., Kelly, D.D., Brutus, M., Mansour, A. & Glusman, M. 2-Deoxy-D-glucose-induced decrements in operant and reflex pain thresholds. *Pharmacol Biochem Behav* **9**, 543-549 (1978).
6. Bodnar, R.J., Kelly, D.D., Spiaggia, A., Ehrenberg, C. & Glusman, M. Dose-dependent reductions by naloxone of analgesia induced by cold-water stress. *Pharmacol Biochem Behav* **8**, 667-672 (1978).
7. Basbaum, A.I. & Fields, H.L. Endogenous pain control mechanisms: review and hypothesis. *Ann Neurol* **4**, 451-462 (1978).
8. Fields, H.L., Heinricher, M.M. & Mason, P. Neurotransmitters in nociceptive modulatory circuits. *Annu Rev Neurosci* **14**, 219-245 (1991).
9. Heinricher, M.M., Tavares, I., Leith, J.L. & Lumb, B.M. Descending control of nociception: Specificity, recruitment and plasticity. *Brain Res Rev* **60**, 214-225 (2009).
10. Zhang, Y.*, et al.* Identifying local and descending inputs for primary sensory neurons. *J Clin Invest* **125**, 3782-3794 (2015).
11. Borsook, D. Pain: the past, present and future. *Adv Drug Deliv Rev* **55**, 931-934 (2003).
12. Rodriguez, E.*, et al.* A craniofacial-specific monosynaptic circuit enables heightened affective pain. *Nat Neurosci* **20**, 1734-1743 (2017).
13. Barik, A., Thompson, J.H., Seltzer, M., Ghitani, N. & Chesler, A.T. A Brainstem-Spinal Circuit Controlling Nocifensive Behavior. *Neuron* **100**, 1491-1503 e1493 (2018).
14. Campos, C.A., Bowen, A.J., Roman, C.W. & Palmiter, R.D. Encoding of danger by parabrachial CGRP neurons. *Nature* **555**, 617-622 (2018).
15. Bernard, J.F. & Besson, J.M. The spino(trigemino)pontoamygdaloid pathway: electrophysiological evidence for an involvement in pain processes. *J Neurophysiol* **63**, 473-490 (1990).
16. Han, S., Soleiman, M.T., Soden, M.E., Zweifel, L.S. & Palmiter, R.D. Elucidating an Affective Pain Circuit that Creates a Threat Memory. *Cell* **162**, 363-374 (2015).
17. Chiang, M.C.*, et al.* Divergent Neural Pathways Emanating from the Lateral Parabrachial Nucleus Mediate Distinct Components of the Pain Response. *Neuron* (2020).
18. Hirschberg, S., Li, Y., Randall, A., Kremer, E.J. & Pickering, A.E. Functional dichotomy in spinal- vs prefrontal-projecting locus coeruleus modules splits descending noradrenergic analgesia from ascending aversion and anxiety in rats. *Elife* **6**(2017).
19. Jones, S.L. & Gebhart, G.F. Characterization of coeruleospinal inhibition of the nociceptive tail-flick reflex in the rat: mediation by spinal alpha 2-adrenoceptors. *Brain Res* **364**, 315-330 (1986).
20. Francois, A.*, et al.* A Brainstem-Spinal Cord Inhibitory Circuit for Mechanical Pain Modulation by GABA and Enkephalins. *Neuron* **93**, 822-839 e826 (2017).
21. Gebhart, G.F. Descending modulation of pain. *Neurosci Biobehav Rev* **27**, 729-737 (2004).
22. Fields, H.L., Basbaum, A.I., Clanton, C.H. & Anderson, S.D. Nucleus raphe magnus inhibition of spinal cord dorsal horn neurons. *Brain Res* **126**, 441-453 (1977).
23. Le Bars, D. The whole body receptive field of dorsal horn multireceptive neurones. *Brain Res Brain Res Rev* **40**, 29-44 (2002).

24. Bannister, K. & Dickenson, A.H. What the brain tells the spinal cord. *Pain* **157**, 2148-2151 (2016).
25. Le Bars, D., Dickenson, A.H. & Besson, J.M. Diffuse noxious inhibitory controls (DNIC). I. Effects on dorsal horn convergent neurones in the rat. *Pain* **6**, 283-304 (1979).
26. Le Bars, D., Dickenson, A.H. & Besson, J.M. Diffuse noxious inhibitory controls (DNIC). II. Lack of effect on non-convergent neurones, supraspinal involvement and theoretical implications. *Pain* **6**, 305-327 (1979).
27. Ritter, S., Li, A.J., Wang, Q. & Dinh, T.T. Minireview: The value of looking backward: the essential role of the hindbrain in counterregulatory responses to glucose deficit. *Endocrinology* **152**, 4019-4032 (2011).
28. Sawchenko, P.E. & Swanson, L.W. Central noradrenergic pathways for the integration of hypothalamic neuroendocrine and autonomic responses. *Science* **214**, 685-687 (1981).
29. McKellar, S. & Loewy, A.D. Efferent projections of the A1 catecholamine cell group in the rat: an autoradiographic study. *Brain Res* **241**, 11-29 (1982).
30. Woulfe, J.M., Hrycyshyn, A.W. & Flumerfelt, B.A. Collateral axonal projections from the A1 noradrenergic cell group to the paraventricular nucleus and bed nucleus of the stria terminalis in the rat. *Exp Neurol* **102**, 121-124 (1988).
31. Westlund, K.N., Zhang, D., Carlton, S.M., Sorkin, L.S. & Willis, W.D. Noradrenergic innervation of somatosensory thalamus and spinal cord. *Prog Brain Res* **88**, 77-88 (1991).
32. Dogrul, A., Ossipov, M.H. & Porreca, F. Differential mediation of descending pain facilitation and inhibition by spinal 5HT-3 and 5HT-7 receptors. *Brain Res* **1280**, 52-59 (2009).
33. Brenchat, A.*, et al.* 5-HT7 receptor activation inhibits mechanical hypersensitivity secondary to capsaicin sensitization in mice. *Pain* **141**, 239-247 (2009).
34. Gebhart, G.F., Sandkuhler, J., Thalhammer, J.G. & Zimmermann, M. Inhibition of spinal nociceptive information by stimulation in midbrain of the cat is blocked by lidocaine microinjected in nucleus raphe magnus and medullary reticular formation. *J Neurophysiol* **50**, 1446-1459 (1983).
35. Bannister, K., Patel, R., Goncalves, L., Townson, L. & Dickenson, A.H. Diffuse noxious inhibitory controls and nerve injury: restoring an imbalance between descending monoamine inhibitions and facilitations. *Pain* **156**, 1803-1811 (2015).
36. Scherrer, G.*, et al.* Dissociation of the opioid receptor mechanisms that control mechanical and heat pain. *Cell* **137**, 1148-1159 (2009).
37. Cavanaugh, D.J.*, et al.* Distinct subsets of unmyelinated primary sensory fibers mediate behavioral responses to noxious thermal and mechanical stimuli. *Proc Natl Acad Sci U S A* **106**, 9075-9080 (2009).
38. Mishra, S.K., Tisel, S.M., Orestes, P., Bhangoo, S.K. & Hoon, M.A. TRPV1-lineage neurons are required for thermal sensation. *EMBO J* **30**, 582-593 (2011).
39. Cui, L.*, et al.* Identification of Early RET+ Deep Dorsal Spinal Cord Interneurons in Gating Pain. *Neuron* **91**, 1413 (2016).
40. Duan, B.*, et al.* Identification of spinal circuits transmitting and gating mechanical pain. *Cell* **159**, 1417-1432 (2014).
41. Peirs, C.*, et al.* Dorsal Horn Circuits for Persistent Mechanical Pain. *Neuron* **87**, 797-812 (2015).
42. Petitjean, H.*, et al.* Dorsal Horn Parvalbumin Neurons Are Gate-Keepers of Touch-Evoked Pain after Nerve Injury. *Cell Rep* **13**, 1246-1257 (2015).
43. Samineni, V.K.*, et al.* Divergent Modulation of Nociception by Glutamatergic and GABAergic Neuronal Subpopulations in the Periaqueductal Gray. *eNeuro* **4**(2017).
44. Liu, Y.*, et al.* Touch and tactile neuropathic pain sensitivity are set by corticospinal projections. *Nature* **561**, 547-550 (2018).

45. Sladek, C.D. Vasopressin response to osmotic and hemodynamic stress: neurotransmitter involvement. *Stress* **7**, 85-90 (2004).
46. Pacak, K. Stressor-specific activation of the hypothalamic-pituitary-adrenocortical axis. *Physiol Res* **49 Suppl 1**, S11-17 (2000).
47. Li, A.J., Wang, Q., Dinh, T.T. & Ritter, S. Simultaneous silencing of Npy and Dbh expression in hindbrain A1/C1 catecholamine cells suppresses glucoprivic feeding. *J Neurosci* **29**, 280-287 (2009).
48. Crane, J.W., French, K.R. & Buller, K.M. Patterns of neuronal activation in the rat brain and spinal cord in response to increasing durations of restraint stress. *Stress* **8**, 199-211 (2005).
49. Dayas, C.V., Buller, K.M. & Day, T.A. Hypothalamic paraventricular nucleus neurons regulate medullary catecholamine cell responses to restraint stress. *J Comp Neurol* **478**, 22-34 (2004).
50. Chance, W.T. The role of brain and spinal cord norepinephrine in autoanalgesia. *Ann N Y Acad Sci* **467**, 309-330 (1986).
51. Yarnitsky, D. Conditioned pain modulation (the diffuse noxious inhibitory control-like effect): its relevance for acute and chronic pain states. *Curr Opin Anaesthesiol* **23**, 611-615 (2010).
52. Yarnitsky, D., Granot, M., Nahman-Averbuch, H., Khamaisi, M. & Granovsky, Y. Conditioned pain modulation predicts duloxetine efficacy in painful diabetic neuropathy. *Pain* **153**, 1193-1198 (2012).
53. Niesters, M.*, et al.* Tapentadol potentiates descending pain inhibition in chronic pain patients with diabetic polyneuropathy. *Br J Anaesth* **113**, 148-156 (2014).
54. Perrotta, A.*, et al.* Facilitated temporal processing of pain and defective supraspinal control of pain in cluster headache. *Pain* **154**, 1325-1332 (2013).
55. Nir, R.R. & Yarnitsky, D. Conditioned pain modulation. *Curr Opin Support Palliat Care* **9**, 131-137 (2015).
56. Sandrini, G.*, et al.* Abnormal modulatory influence of diffuse noxious inhibitory controls in migraine and chronic tension-type headache patients. *Cephalalgia* **26**, 782-789 (2006).
57. Pielsticker, A., Haag, G., Zaudig, M. & Lautenbacher, S. Impairment of pain inhibition in chronic tension-type headache. *Pain* **118**, 215-223 (2005).
58. Petersen, K.K., Arendt-Nielsen, L., Simonsen, O., Wilder-Smith, O. & Laursen, M.B. Presurgical assessment of temporal summation of pain predicts the development of chronic postoperative pain 12 months after total knee replacement. *Pain* **156**, 55-61 (2015).
59. Beas, B.S.*, et al.* The locus coeruleus drives disinhibition in the midline thalamus via a dopaminergic mechanism. *Nat Neurosci* **21**, 963-973 (2018).
60. Brenner, D.S., Golden, J.P. & Gereau, R.W.t. A novel behavioral assay for measuring cold sensation in mice. *PLoS One* **7**, e39765 (2012).
61. Mishra, S.K. & Hoon, M.A. The cells and circuitry for itch responses in mice. *Science* **340**, 968-971 (2013).

Figures

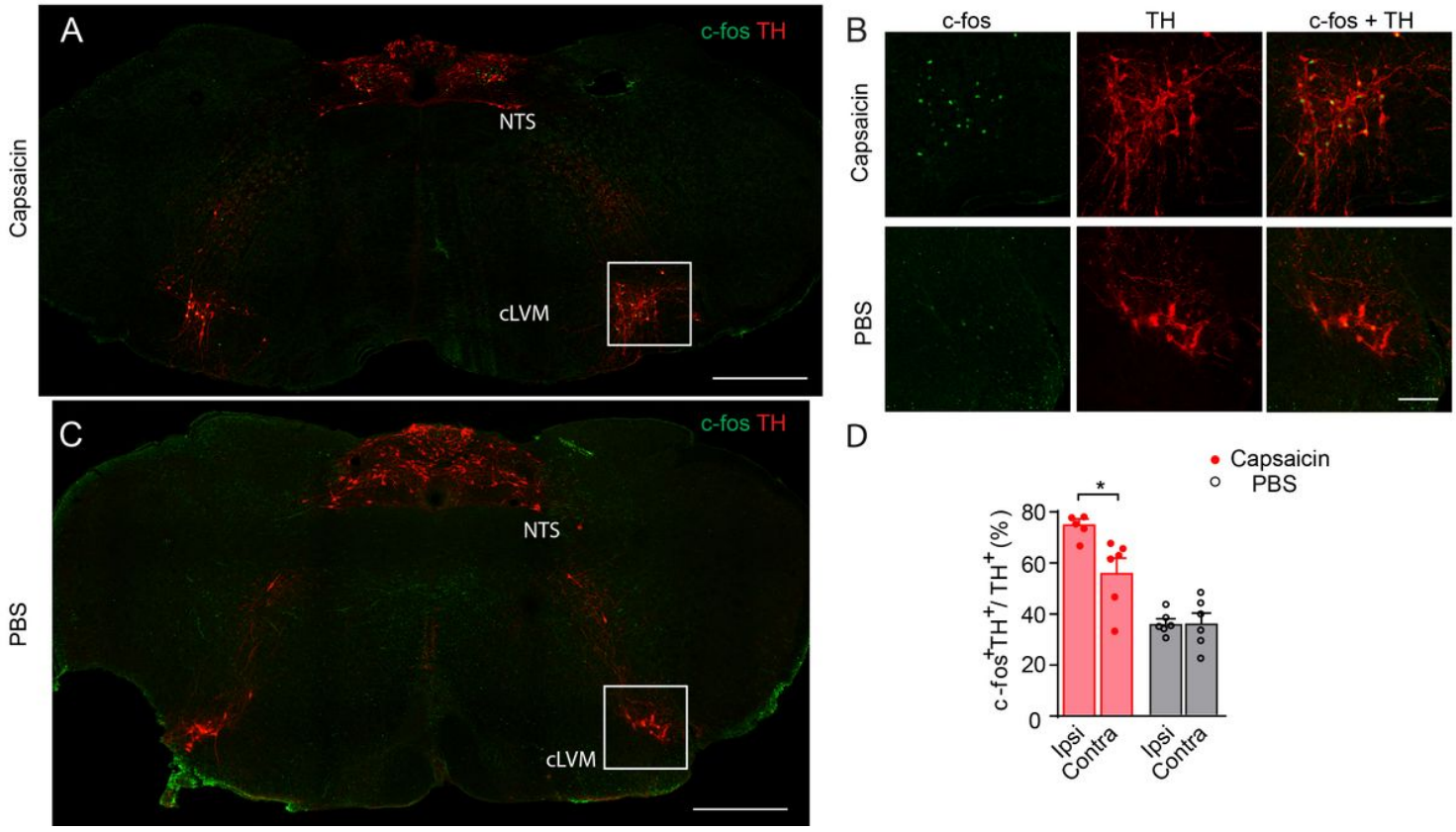

Figure 1

The cVLMTH, a brainstem nucleus activated by capsaicin. A-C. Immunostaining for cfos in the caudal medulla of mice injected into the hind-paw unilaterally with capsaicin (A) or with saline (C) revealed that nociceptive stimulation increased numbers of TH+ neurons positive for cfos in the cVLM. B. Magnified view (see boxed area in A and C) of the cVLM showed that almost all TH-labeled neurons were cfospositive after administration of capsaicin and few TH-neurons were cfos-labeled after saline treatment ($p=<0.001$, n=6 mice). D. The increase in the percent of cfos+TH+ to TH+ neurons was more in the ipsilateral cVLM compared to contralateral side $p<0.010$, n=6 mice, Student T-test, data represent means ± SEM (Capsaicin ipsilateral 341/452, Capsaicin contralateral 219/404, PBS ipsilateral 154/440, PBS contralateral 147/371). Scale bars: 500 µm for coronal sections and 50 µm for magnified field images.

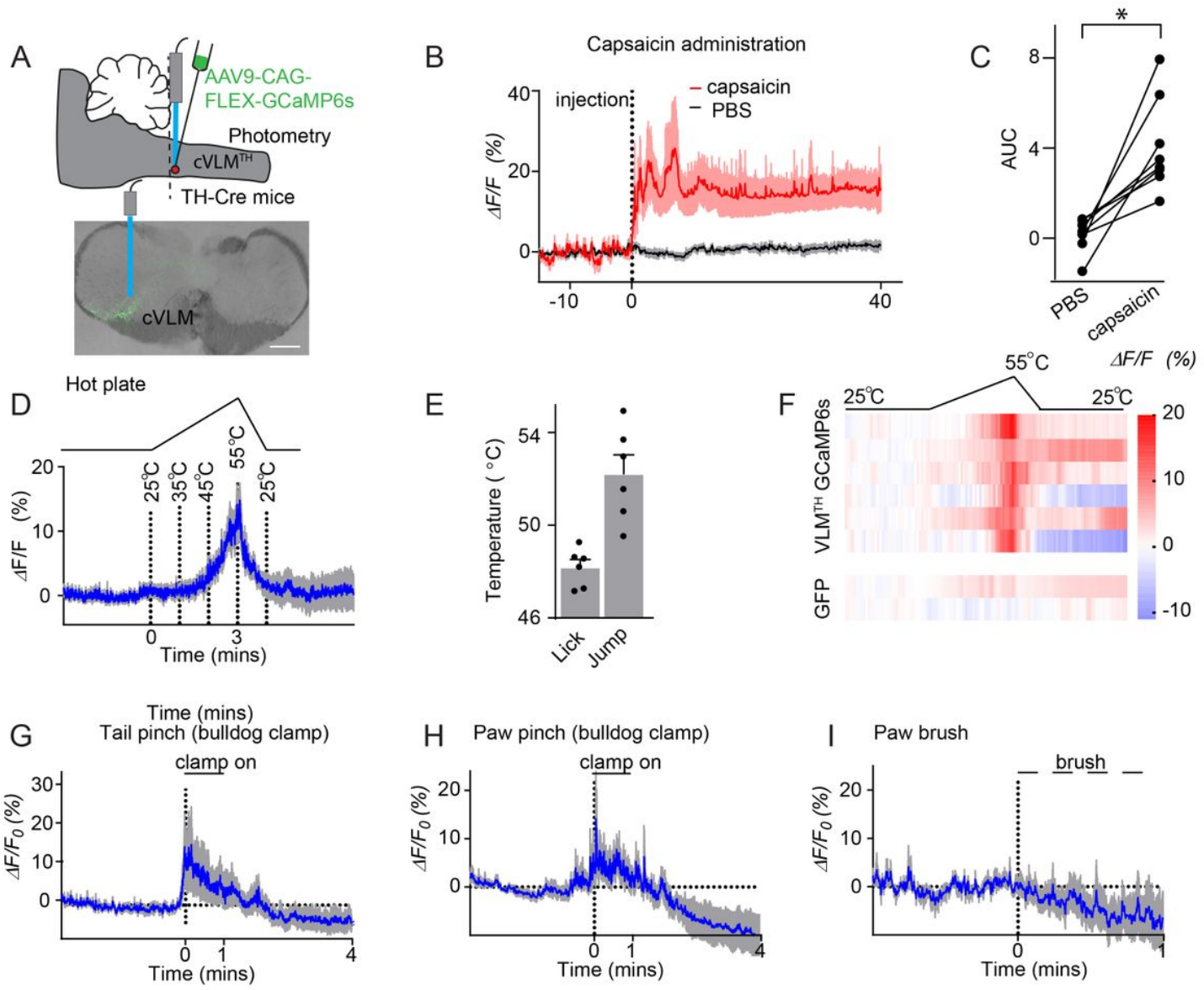

Figure 2

cVLMTH-neurons are activated by noxious stimuli. A. Schematic of the procedures used to probe intracellular calcium responses of cVLMTH-neurons and a representative image (approx. position shown by dotted line) of GCaMP6s expression (lower panel). B. Averaged in vivo fiber photometry results from cVLMTH-neurons upon stimulation with capsaicin (red; injected into hind-paw) and saline (grey), n=8 mice, data are represented as mean results (red) ± SEM (shadow). C. Area under the curve (AUC) quantification showed that capsaicin treatment significantly increased calcium responses; p=0.0307, n=8 mice, Student paired T-test, data represent means ± SEM. D. Responses to heat challenge on a hot plate show intracellular calcium increased in cVLMTH-neurons in the noxious temperature range, n=6 mice. Hot plate 7 temperature linearly increased from 25°C to 55°C in 3 min. E. Nociceptive behavioral reaction coincided with increased calcium levels. F. Heatmap traces from 6 individual animals to heat challenge compared to those observed in GFP-expressing control animals (lower two traces). G-I. Calcium responses to bulldog pinch to the tail and hindpaw, and the fine brush stimulation of hind-paw respectively, averaged responses (blue) ± SEM (grey) n=6 mice.

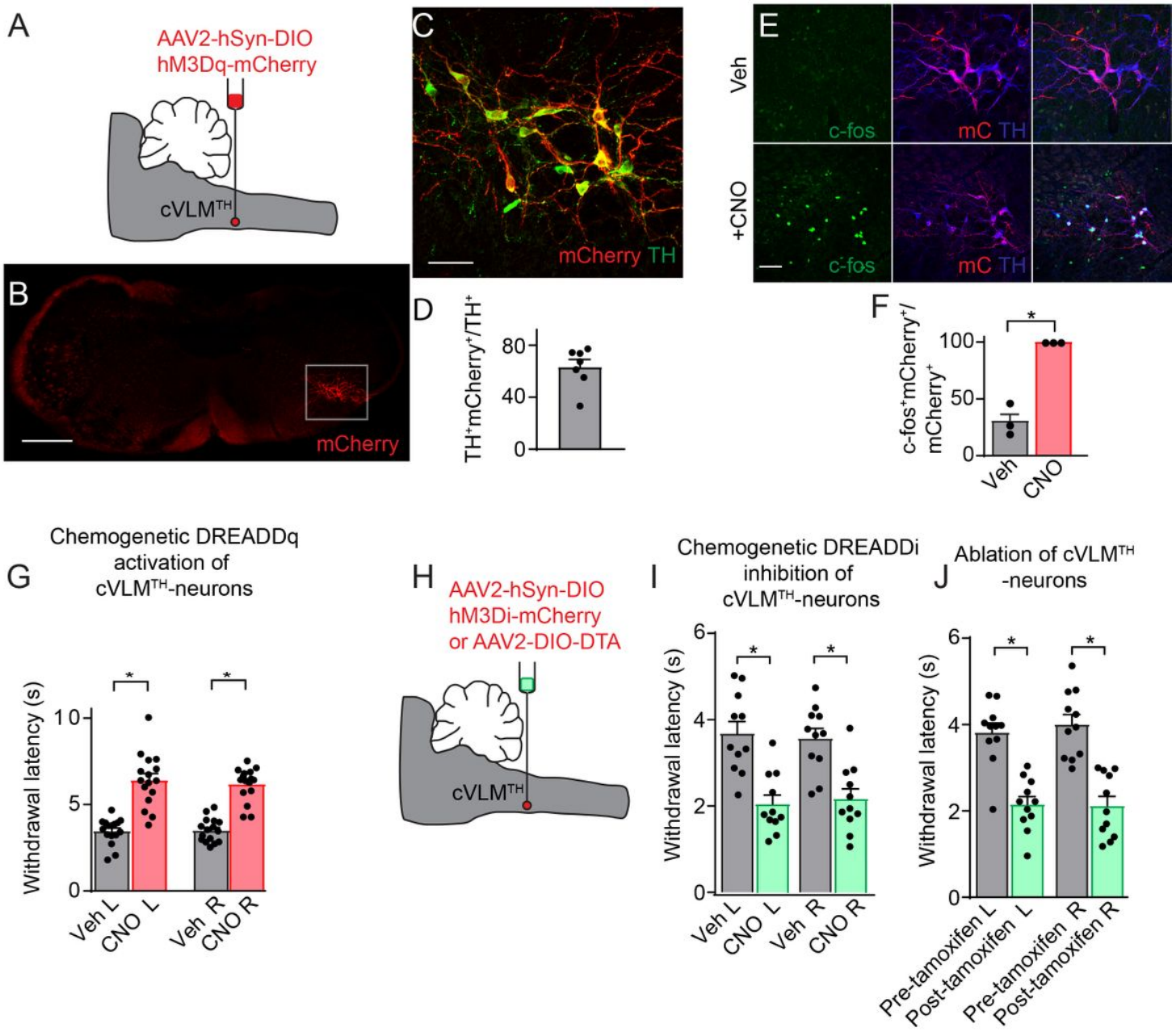

Figure 3

VLMTH-neurons potently control nociceptive behavioral responses. A Schematic of the strategy employed to chemogenetically stimulate cVLMTH-neurons. B. Representative image showing the neurons expressing DREADDq-mCherry in the cVLM. C. Magnified view (boxed area in B) displaying that all mCherry expressing neurons are TH-positive. D. Quantification of the numbers of TH-neurons expressing mCherry, n=7 mice, data represent means ± SEM (mCherry+TH+/TH+=177/281). E. Upon addition of CNO (lower panels), DREADDq stimulation led to cfos expression in TH+-immunostained neurons. F. Quantification of the percentage of TH-neurons expressing cfos (Veh, cfos+mCherry/mCherry+=21/75, CNO, cfos+mCherry/mCherry+= 83/83). G. Withdrawal latencies were significantly increased, in Hargreaves tests, for mice where CNO was used to stimulate DREADDq in cVLMTH-neurons compared to saline injected mice (L and R indicate left and right hind-paw respectively), n=16, $p<0.001$, Student T-test.

H. Schematic of the strategy employed to chemogenetically inhibit cVLMTH-neurons. I. Chemogenetic inhibition with DREADDi caused a significant shortening of withdrawal latencies compared to saline controls, n=11, p<0.001, Student T-test. J. Diphtheria toxin subunit A was expressed, after tamoxifen induction, in cVLM TH-neurons of TH-CreER mice. Ablation of cVLMTH-neurons caused a significant shortening of withdrawal latencies compared to saline controls, n=11, p<0.001, Student T-test.

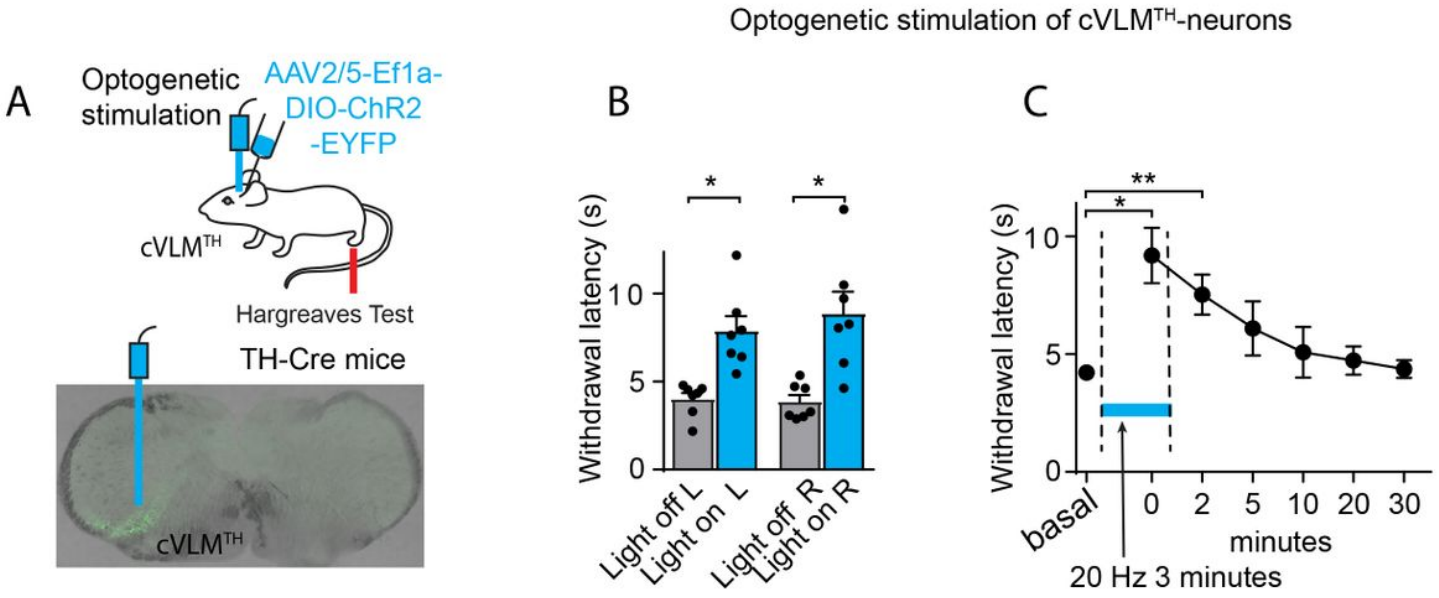

Figure 4

Optogenetic stimulation of cVLMTH triggers extended suppression of nociceptive responses. A. Schematic of the strategy used to stimulate cVLMTH-neurons and representative image of ChR2 expression in the cVLM. B. Optogenetic stimulation caused a significant increase in withdrawal latencies in Hargreaves assays, compared to baseline, n=7, p<0.05 for L hindpaw and p<0.01 for R hind-paw, Student T-test, data represent means ± SEM. C. Timecourse for activation and deactivation of attenuated responses to heat challenge (Hargreaves test) following optogenetic stimulation; testing was performed prior to, during (blue line), and after optogenetic stimulation. There was a significant difference in withdrawal responses compared to baseline during stimulation and at 2 min after the end of optogenetic stimulation, p=0.025 and p=0.021 respectively, n=7, Dunnett's tests following One-Way ANOVA.

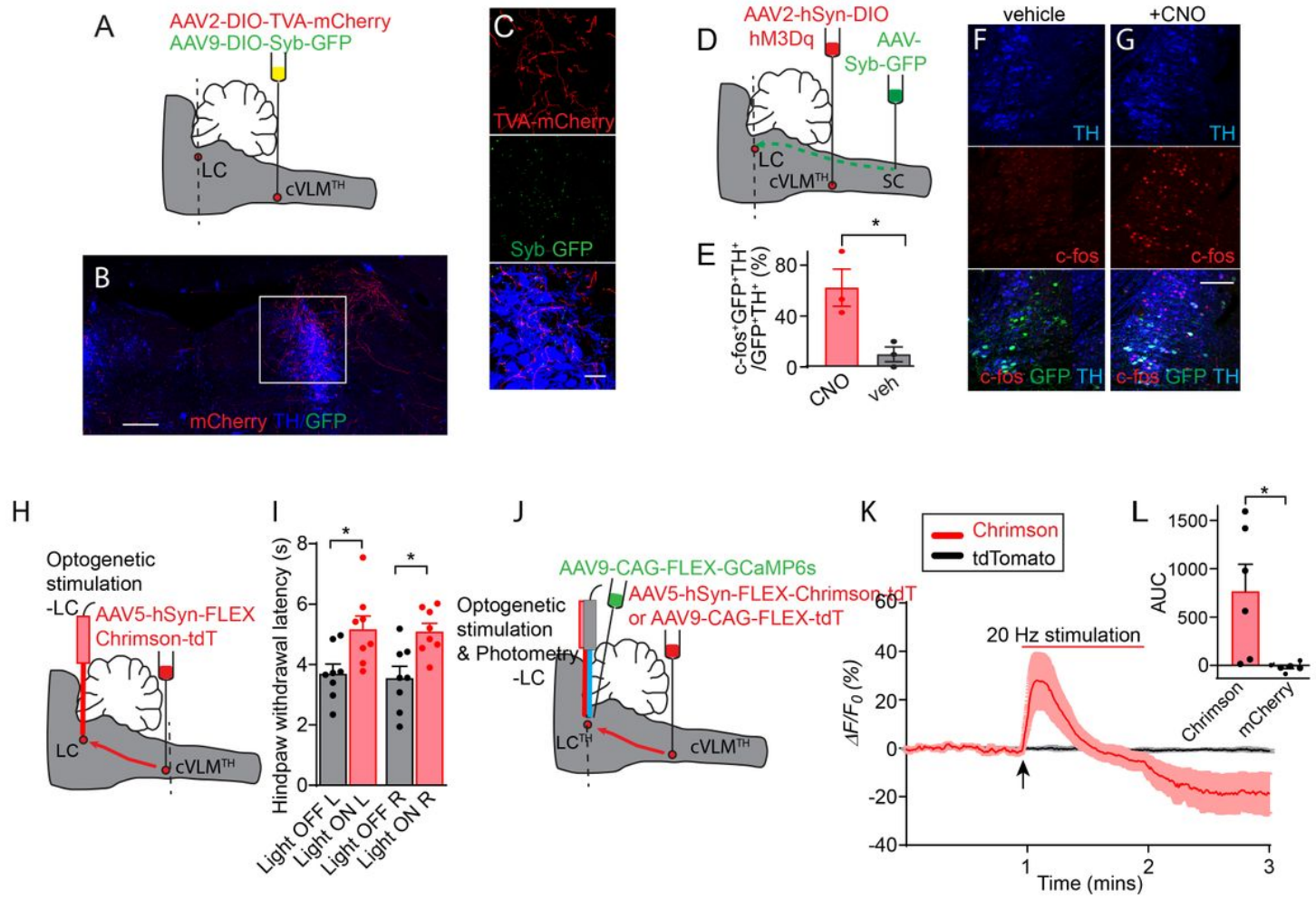

Figure 5

A descending antinociceptive cVLM-LC-spinal cord circuit. A. Scheme showing the procedure used to identify synaptic partners of cVLMTHneurons. B. Representative image of a section of the hindbrain (approx. position shown by dotted line A.) showing labeled fibers (red) and synaptic boutons (green) of cVLMTHneurons. C. Magnified view of boxed area (in B). D. Strategy employed to stimulate cVLMTH-neurons and to label LC neurons projecting to the SC. E. Quantification of numbers of LC neurons projecting to the SC (GFP+TH+) which were cfos positive (cfos+GFP+TH+) revealed a significant increase upon DREADDq stimulation (CNO) compared to saline control, n=3 mice, p=0.029, Student T-test, data represent means ± SEM (CNO, cfos+GFP+TH+/GFP+TH+ = 32/65, Veh, cfos+GFP+TH+/GFP+TH+=3/30). F-G. Representative images of LC sections (approx. position shown by dotted line (D.) for mice administered vehicle (F.) or CNO (G.) showed an increase in cfos (red) labeling 12 in spinal cord projecting neuronsfollowing chemogenetic activation of cVLMTHneurons. H. Diagram of the approach used to optogenetically activate LC-projecting cVLMTH-neuronal fibers. I. Optogenetic stimulation caused a significant increase in withdrawal latencies in left (L) and right (R) hind-paws, in Hargreaves assays, compared to baseline, n = 8, p=0.0097 for left and 0.0196 for right hind-paws, paired Student Ttest, data represent means ± SEM. J. Diagram of the approach used to optogenetically activate LC-projecting cVLMTH-neuronal fibers in conjunction with record calcium responses in LC-neurons. K. Measurement of

calcium responses in LC-neurons using in vivo fiber photometry showed that stimulation of LC projecting cVLMTH-neuronal fibers rapidly increases intracellular calcium in LC neurons, data are represented as mean results (red or black line) ± SEM (pink or grey). L. Quantification of area under the curve (AUC) responses show that activation of Chrimson expressing fibers produces significantly more responses compared to tdTomato-expressing fibers, n=6, p=0.0168 Student t-test, data represent means ± SEM. Scale bars: 500 µm in B, H and J; 50 µm in C, 100 µm in F and G.

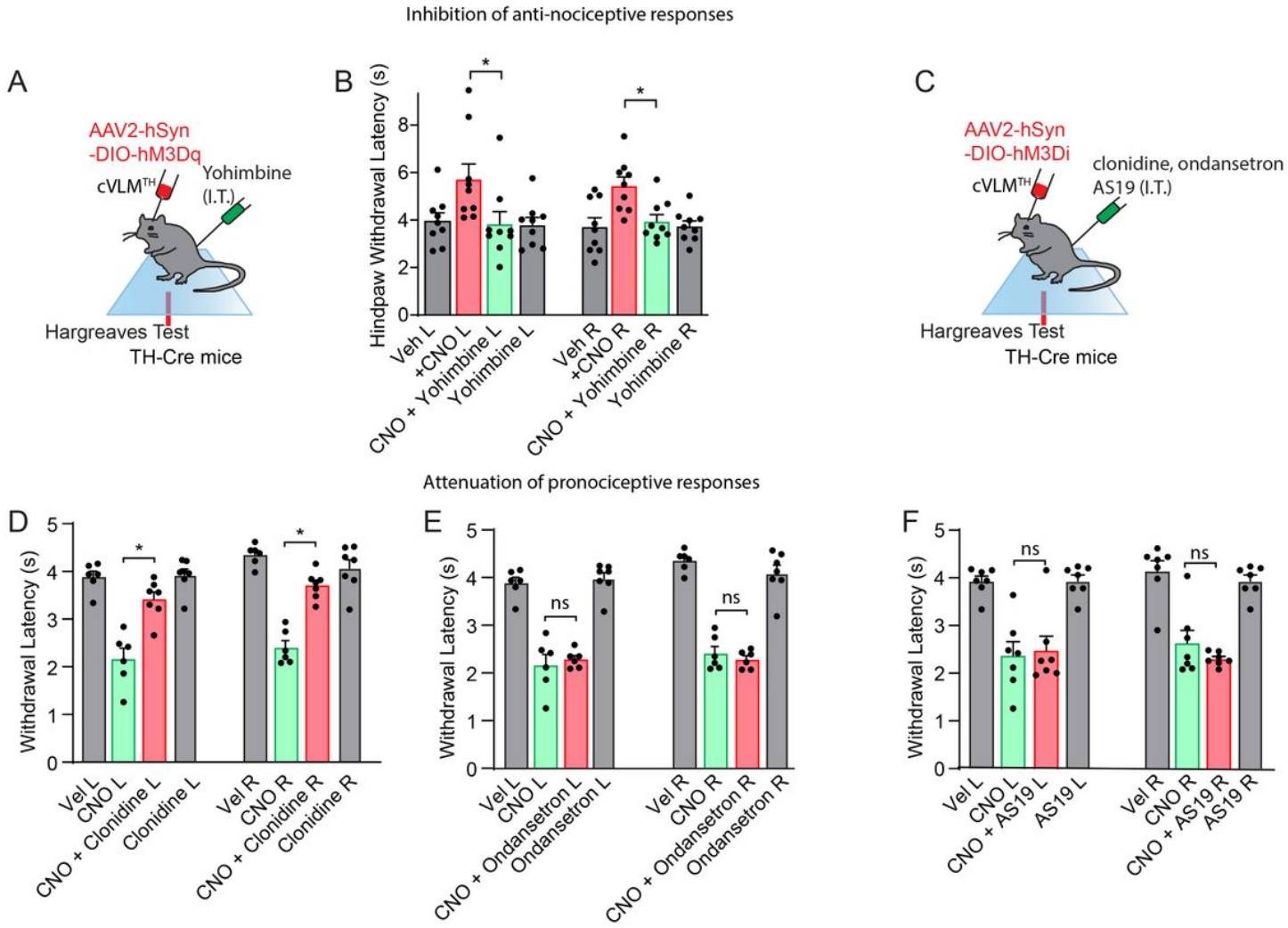

Figure 6

Antinociceptive and pronociceptive responses induced by cVLMTH-neurons are disrupted by spinal cord administration of α2-adrenergic receptor antagonist and agonist respectively. A. Experimental paradigm used to examine the influence of spinal cord noradrenalin on cVLMTH-neuron induced antinociceptive effects. B. Chemogenetic activation (DREADDq) of cVLMTH-neuron induces increased withdrawal latencies in Hargreaves test which were significantly attenuated by intrathecal administration of yohimbine, n=9, p=0.050 for L and 0.018 for R hind-paws respectively, Student T-test, data represent means ± SEM. C. Chemogenetic inhibition (DREADDi) of cVLMTH-neurons produced pronoception likely through adrenergic modulation. D. Intrathecal injection of the α2-adrenergic agonist, clonidine, reversed the CNO-induced sensitization of hind-paw responses measured with the Hargreaves tests, n = 7, p

<0.001, for both L and R hind-paws, paired Student T-test, data 15 represent means ± SEM. E. By contrast, the serotonin 5-hydroytryptamine type 3 (5-HT3) receptor antagonist ondansetron (suggested to be responsible, in part, for descending facilitation of pain from the RVM) had no effect on CNO-induced hyperalgesia, n=7, p=0.578 for L (left) and p=0.341 for R (right) hind-paws. F. Similarly, 5-hydroytryptamine type 7 (5-HT7) receptor agonist, AS19 (thought to be responsible, in part, for the descending inhibition of pain from the RVM) also did not affect CNO-induced hyperalgesia, n=7, p=0.858 for L and p=0.363 for R hind-paws, paired Student T-test, data represent means ± SEM.

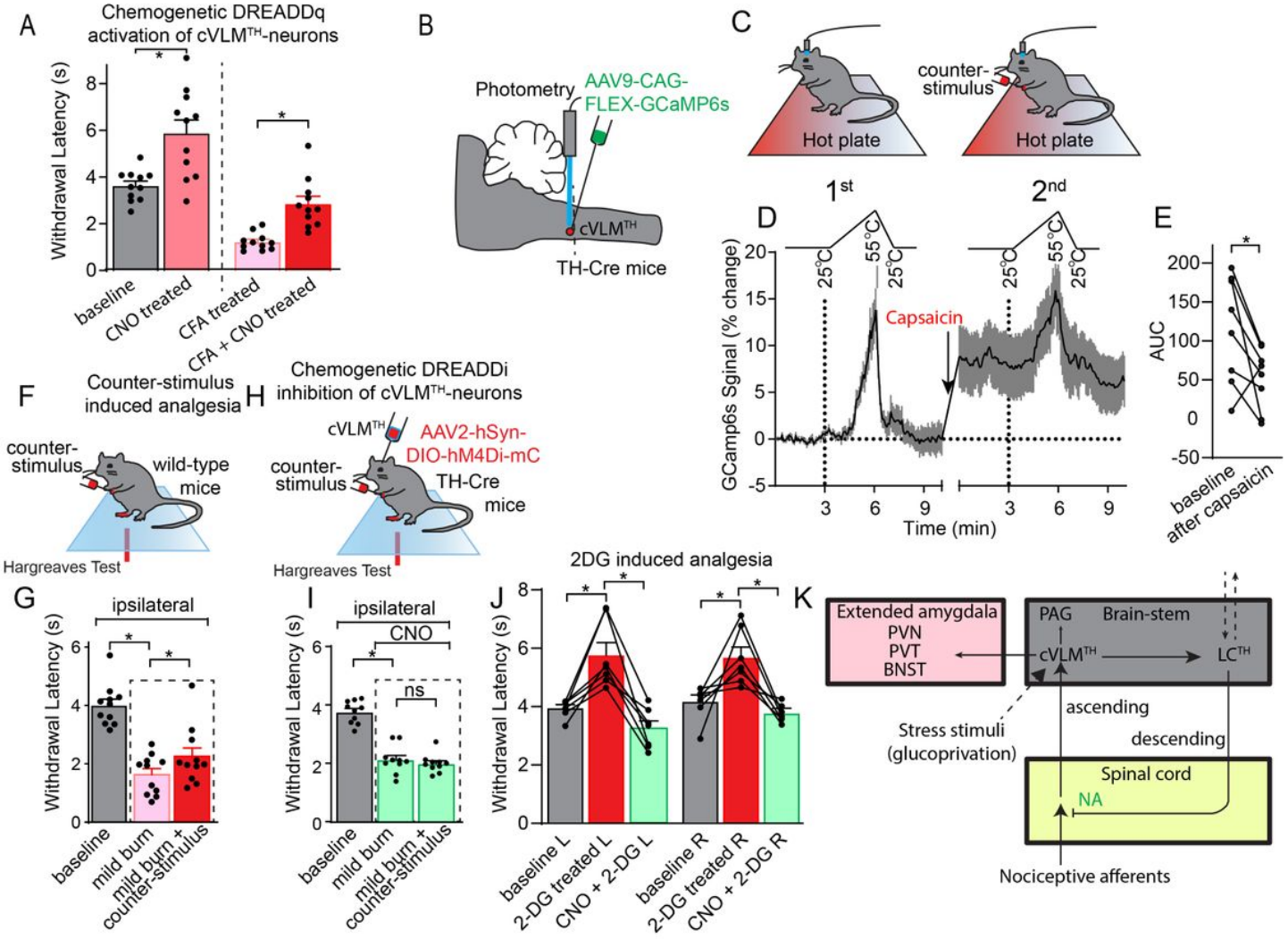

Figure 7

The cVLM-circuit is required and sufficient for counter-stimulus induced analgesia. A Chemogenetic activation of cVLMTH-neurons significantly lengthens withdrawal latencies to heat stimulation after inflammation (complete Freuds Adjuvant (CFA)), n=11 mice, p<0.001 Student T-test, data represent means ± SEM. BC. Schematic of procedures used to record changes in intracellular calcium in cVLMTH-neurons and the experimental design used to examine the effects of counter-stimulation on responses to hot plate temperature ramps; mice were tested three times (1st) with 55 ºC ramps, mice were given a 1-hour rest and then injected with capsaicin (as indicated). Next, a further three heat ramps trials were performed (2nd). D. Averaged responses over trials before and after counter-stimulation showed that

responses to individual ramps were diminished after capsaicin treatment, data 18 are represented as mean results (black line) ± SEM (grey). E. Quantification of area under the curve (AUC) for responses to heat ramps were significantly reduced after capsaicin treatment, n=8 mice, p=0.033 Student T-test, data represent means ± SEM. F. Scheme showing the experimental design for measurement of counter-stimulus induced analgesia; one hind-paw received a mild-burn (ipsilateral) and withdrawal latencies were determined using the Hargreaves test before and after capsaicin injection into a forepaw. G. Latencies for withdrawal of the ipsilateral paw were significantly reduced compared to baseline after mild burn and were significantly increased compared to mild-burn after administration of counter stimulus, n=11 mice, p=<0.0010.0001 and p=0.035 respectively, Student paired Ttest, data represent means ± SEM. H. Diagram depicting the approach used to determine the effect of cVLMTH-circuit on counter-stimulus induced analgesia. I. Chemogenetic inhibition of cVLMTH-neurons prevented attenuation of counter-stimulation (capsaicin) induced analgesia of the ipsilateral paw, p=0.121, while mild-burn was significantly reduced compared to baseline p=<0.001, n=10 mice, Student T-test, data represent means ± SEM. J. Chemogenetic inhibition of cVLMTH-neurons prevented 2DG induced analgesia. Hargreaves withdrawal responses were significant longer after 2DG treatment compared to baseline, p=0.005 and p=0.023 for left (L) and right R paws respectively, and 2DG responses were significantly reduced compared to chemogenetic inhibition (CNO), p=0.001 and p=0.003 for L and R paws respectively, n=7 mice, Student T-test, data represent means ± SEM. K. Proposed model for feed-forward inhibition by the cVLM-circuit.

Supplementary Files

This is a list of supplementary files associated with this preprint. Click to download.

- FigureS1NN.jpg
- FigureS2.jpg
- FigureS3.jpg
- FigureS4.jpg
- FigureS5.jpg
- FigureS6.jpg
- FigureS7.jpg
- SuplementsNN.pdf
- FigureS8.jpg